Source and H2O content of high-MgO magmas in island arc settings - An experimental study on primitive calk-alkaline basalts from St. Vincent, Lesser Antilles.

Michel Pichavant, B. O. Mysen, Ray Macdonald

Pergamon

Geochimica et Cosmochimica Acta, Vol. 66, No. 12, pp. 2193–2209, 2002

0016-7037/02 $22.00 + .00

PII S0016-7037(01)00891-2

Source and H_2O content of high-MgO magmas in island arc settings: An experimental study of a primitive calc-alkaline basalt from St. Vincent, Lesser Antilles arc

M. PICHAVANT,[1,*] B. O. MYSEN,[2] and R. MACDONALD[3]

[1]Institut des Sciences de la Terre d'Orléans (ISTO), UMR 6113 CNRS-UO, 1A rue de la Férollerie, 45071 Orléans, France
[2]Geophysical Laboratory, Carnegie Institution of Washington, 5251 Broad Branch Road, NW, Washington, DC 20015-1305, USA
[3]Environmental Science Division, IENS, Lancaster University, Lancaster LA1 4YQ, UK

(*Received June* 6, 2001; *accepted in revised form November* 28, 2001)

Abstract—Liquidus phase relationships have been determined for a high-MgO basalt (STV301: MgO=12.5 wt%, Ni=250 ppm, Cr=728 ppm) from Black Point, St Vincent (Lesser Antilles arc). Piston-cylinder experiments were conducted between 7.5 and 20 kbar under both hydrous and oxidizing conditions. AuPd capsules were used as containers. Compositions of supraliquidus glasses and mass-balance calculations show that Fe loss is $<$ 10% in the majority of experiments. Two series of water concentrations in melt were investigated: (i) 1.5 wt% and (ii) 4.5 wt% H_2O, as determined by SIMS analyses on quenched glasses and with the by difference technique. The Fe^{3+}/Fe^{2+} partitioning between Cr-Al spinel and melt and olivine-spinel equilibria show that oxidizing fO_2 were imposed (NNO + 1.5 for the 1.5 wt% H_2O series, NNO + 2.3 for the 4.5 wt% H_2O series). For both series of water concentrations, the liquid is multiply-saturated with a spinel lherzolite phase assemblage on its liquidus, at 1235°C, 11.5 kbar (1.5 wt% H_2O) and 1185°C, 16 kbar (4.5 wt% H_2O). Liquidus phases are homogeneous and comparable to typical mantle compositions. Mineral-melt partition coefficients are generally identical to values under anhydrous conditions. The modal proportion cpx/opx on the liquidus decreases from the 1.5 wt% to the 4.5 wt% H_2O series. The experimental data are consistent with STV301 being a product of partial melting of lherzolitic mantle. Conditions of multiple saturation progressively evolve toward lower temperatures and higher pressures with increasing melt H_2O concentration. Phase equilibria constraints, i.e., the necessity of preserving the mantle signature seen in high-MgO and picritic arc basalts, and glass inclusion data suggest that STV301 was extracted relatively dry ($\sim$ 2 wt% H_2O) from its mantle source. However, not all primary arc basalts are extracted under similarly dry conditions because more hydrous melts will crystallize during ascent and will not be present unmodified at the surface. From degrees of melting calculated from experiments on KLB-1, extraction of a 12.5 wt% MgO melt with $\sim$ 2 wt% H_2O would require a H_2O concentration of 0.3 wt% in the sub-arc mantle. For mantle sources fluxed with a slab-derived hydrous component, extracted melts may contain up to $\sim$ 5.5 wt% H_2O.

1. INTRODUCTION

High-MgO (MgO $\geq$ 8 wt.%) basalts are relatively uncommon in modern subduction zone settings. Nevertheless, they occur in virtually every island arc and are of great petrological significance as these basalts possibly represent one type of primary magma in subduction zones (e.g., Tatsumi and Eggins, 1995 and references therein). As such, they constitute valuable sources of information on the conditions of partial melting and the thermal structure of the mantle wedge beneath island arcs. In addition, knowledge of the H_2O content of primary arc magmas is important in assessing processes of volatile and material recycling in subduction zones.

Information on the conditions of genesis of high-MgO arc basalts has come mainly from experimental studies. Yet, till now, most high-pressure experimental studies on high-MgO arc basalts have been performed under anhydrous conditions (Tatsumi, 1982; Tatsumi et al., 1983; Gust and Perfit, 1987; Kushiro, 1987; Bartels et al., 1991; Draper and Johnson, 1992; Baker et al., 1994; Tatsumi et al., 1994). Water-bearing experiments have been carried out in only three studies (Tatsumi, 1982; Tatsumi et al. 1983; Baker et al., 1994). Another characteristic of those experiments is that experimental fO_2 conditions generally have been too reducing for arc settings (Tatsumi, 1982; Tatsumi et al., 1983; Gust and Perfit, 1987; Bartels et al., 1991; Draper and Johnson, 1992). Consequently, only a very limited number of experimental studies are truly applicable to real conditions of basaltic melt generation in subduction zones.

The Lesser Antilles intraoceanic island arc is the surface manifestation of the subduction of the American plate beneath the Caribbean plate (Fig. 1). The arc contains a wide range of magma types (Brown et al., 1977; Macdonald et al., 2000), from low-K tholeiites (north), calc-alkaline basalts (central islands) to alkalic basalts in Grenada (south). Primitive, high-MgO and picritic basalts occur mainly in the central and southern parts of the arc. The Soufriere volcano in the northern part of the island of St Vincent is composed almost entirely of calc-alkaline basalts and basaltic andesites (Heath et al., 1998). The most magnesian basalts from Soufriere, St Vincent, resemble high-MgO and picritic basalts known in other arcs, for example Vanuatu (Eggins, 1993), NE Japan (Kushiro, 1987; Tatsumi et al., 1994) and the Aleutians (Nye and Reid, 1986; Draper and Johnson, 1992). Heath et al. (1998) have argued that the high-MgO basalts exposed at St Vincent represent primary mantle-derived magmas and are parental to the

* Author to whom correspondence should be addressed (pichavant@cnrs-orleans.fr).

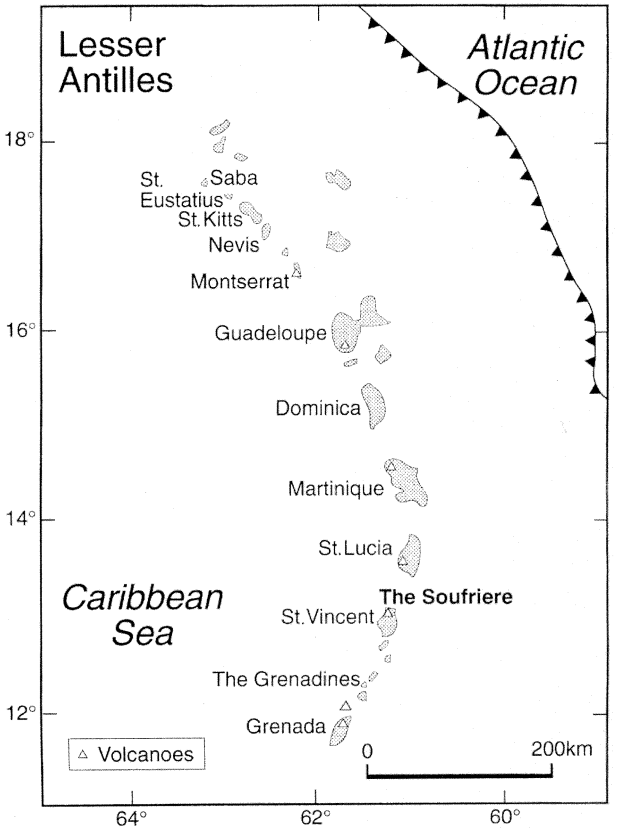

Fig. 1. Map of the Lesser Antilles island arc showing location of the Soufriere volcano, St. Vincent.

andesites which dominate the eruption products in the central and northern parts of the arc. Therefore, these basalts shed light on the origin of the calc-alkaline igneous suite in the Lesser Antilles arc.

In this paper, we present a high-pressure experimental study of a sample of primitive calc-alkaline basalt from Soufriere, St Vincent. The experiments were designed (1) to test whether the composition studied is representative of a primary mantle melt; (2) to determine the effect of H_2O on the pressure-temperature conditions of equilibration of the basaltic liquid with its inferred mantle source; and (3) to provide constraints on the H_2O content of primitive arc magmas.

2. HIGH-MGO BASALTS FROM SOUFRIERE, ST. VINCENT

At Soufriere, St Vincent, both basalts and basaltic andesites have erupted throughout the volcano's history, although basalts were volumetrically the most abundant in the earlier stages (Pre-Somma Lavas and Yellow Tuff Formation, see Heath et al., 1998). The basalts range from microphyric fine-grained rocks with abundant (up to 30%) microphenocrysts of olivine (ol), spinel (sp) and clinopyroxene (cpx), to more coarsely porphyritic rocks also containing phenocrystic plagioclase (pl). Olivines up to $Fo_{89.7}$ can be found (Marcelot et al., 1981; Heath et al., 1998). The ol-sp thermometer of Ballhaus et al. (1991) yields temperatures between 1026 and 1130 °C for these basalts (Heath et al., 1998). The higher end of this range is in agreement with older temperature estimates on the same rocks and likely corresponds to crystallization temperatures (see Heath et al., 1998). The St Vincent basalts record fairly oxidizing redox conditions ($FMQ+1.5 < fO_2 < FMQ+1.8$, Heath et al., 1998).

The most magnesian basaltic lava (STV 301, 12.5 wt.% MgO, Table 1; see also Marcelot et al., 1981) from Black Point is slightly nepheline normative, a feature shared with the silica-undersaturated mafic end-members of the Grenada series (e.g., Thirlwall and Graham, 1984). More evolved St Vincent basalts are silica-oversaturated (Heath et al., 1998). Chondrite-normalized REE patterns for relatively magnesian basalts (Fig. 2) are flat to slightly LREE-enriched. Mantle-normalized element abundances (Fig. 3) show patterns characteristic of arc basalts,

Table 1. Composition of High-MgO Basalt Starting Samples and Glasses.

Sample	STV 301[a] whole-rock	ID 16[b] whole-rock	IK85060803[c] whole-rock	STV 301 glass* (1 atm)	STV 301 glass** (1500°C, 15 kbar)
SiO_2	47.01	48.94	49.03	46.86 (35)	45.89 (27)
TiO_2	1.07	0.70	0.64	1.08 (3)	1.06 (1)
Al_2O_3	15.28	16.01	13.95	15.29 (15)	15.00 (5)
FeO_t	8.79	8.90	8.95	8.96 (17)°	8.71 (14)
MnO	0.16	0.17	0.15	0.17 (3)	0.18 (2)
MgO	12.50	11.42	12.38	11.97 (5)	11.75 (9)
CaO	10.96	10.89	10.75	11.00 (9)	10.71 (13)
Na_2O	2.23	2.21	1.93	2.27 (7)	2.19 (4)
K_2O	0.47	0.52	0.27	0.49 (2)	0.50 (3)
H_2O	nd	nd	1.90	0.10†	2.84†
total	98.47	99.76	99.95	98.19	98.83
Cr	728	662	820	nd	nd
Ni	250	266	nd	nd	nd

[a] Olivine basalt, St. Vincent, Lesser Antilles (Health et al., 1998, this work).
[b] High-magnesia basalt, Umnak, Aleutians (Draper and Johnson, 1992).
[c] Olivine tholeiite, Ryozen, NE Japan (Kushiro, 1987).
* Average of 41 electron microprobe analyses; numbers in brackets are standard deviations in terms of least unit cited.
** Average of 24 electron microprobe analyses; numbers in brackets are standard deviations in terms of least unit cited.
° FeO = 1.52 wt% and Fe_2O_3 = 8.26 wt%; Fe^{3+}/Fe^{2+} (at.) determined by Mössbauer spectroscopy.
† H_2O by Karl-Fischer titration.

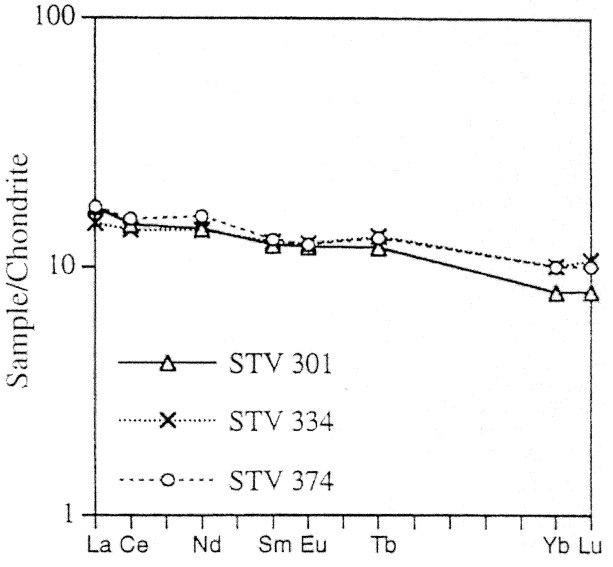

Fig. 2. Chondrite-normalized REE abundances in selected basalts from Soufriere, St Vincent. After Heath et al. (1998).

namely high LILE/HFSE and LREE/HFSE, negative Nb anomalies and relatively high Ba/La. Relative to MORB, the Soufriere basalts show LILE and LREE enrichment and HREE depletion (Fig. 3). The geochemical characteristics of the Soufriere basalts are consistent with generation from a mantle wedge similar to, or slightly enriched in HFSE relative to the midocean ridge basalt (MORB) source, and metasomatized by addition of a fluid phase from the subducting slab (e.g., Heath et al., 1998).

3. EXPERIMENTAL STRATEGY AND METHODS

3.1. Strategy

To test the possible origin of the St Vincent basalt by partial melting of the mantle, the inverse approach was used (e.g., Myers and Johnston, 1996; Falloon et al., 1999). Phase relations were studied near the liquidus of the studied composition by means of high-pressure crystallization experiments. If the studied magma is multiply-saturated with olivine + orthopyroxene (opx) + clinopyroxene on its liquidus, then it is in equilibrium with a lherzolite and is thus considered primary (e.g., Thompson, 1974; Tatsumi et al., 1983, 1994; Kushiro, 1987; Draper and Johnson, 1992; Myers and Johnson, 1996; Falloon et al., 1999). In such a case, the P-T conditions of multiple saturation provide an estimate of the conditions of magma segregation from (or of last equilibration with) its mantle source (e.g., Tatsumi et al., 1983, 1994; Falloon et al., 1999). This conclusion also requires, however, that the phases crystallizing on the liquidus of the study sample have compositions typical of residual upper mantle rocks. Conversely, the absence of multiple saturation with a lherzolite mineral assemblage may indicate either that the composition studied is not a primary mantle melt or that a reaction relationship exists between minerals and melt at the P-T conditions of magma segregation (e.g., Falloon et al., 1999).

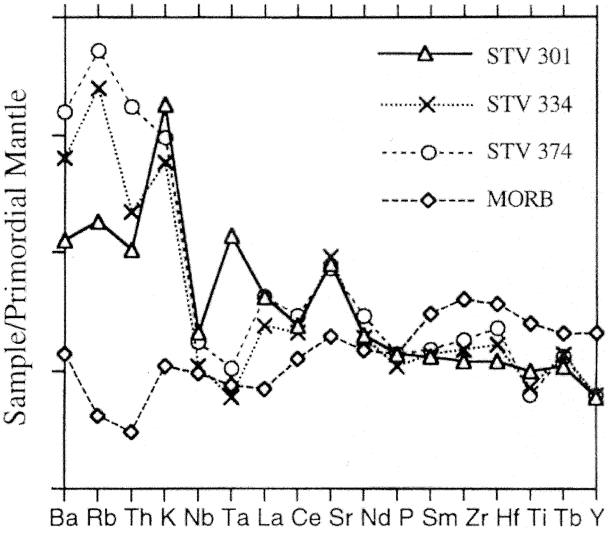

Fig. 3. Primordial mantle-normalized trace element plots for selected basalts, Soufriere, St Vincent, and MORB. After Heath et al. (1998).

Previously, the inverse experimental approach has been applied to several primitive high-MgO arc basalts from NE Japan and the Aleutians (Tatsumi, 1982; Tatsumi et al., 1983; 1994; Gust and Perfit, 1987; Kushiro, 1987; Draper and Johnson, 1992) and to a primitive high-alumina basalt from the Cascades (Bartels et al. 1991). Under anhydrous conditions, several were shown to be multiply-saturated with mantle mineral assemblages on their liquidus, in most cases between 1300 to 1350°C and 10 to 12 kbar (e.g., Kushiro, 1987; Tatsumi et al., 1994). Other high-MgO basalt compositions were shown not to be multiply-saturated with a lherzolitic mantle assemblage on their liquidus (Gust and Perfit, 1987; Bartels et al., 1991; Falloon et al., 1999). The few data available under hydrous conditions (Tatsumi, 1982; Tatsumi et al., 1983) show that the effect of water is to shift the P-T conditions of multiple saturation towards lower temperatures and higher pressures. However, H_2O concentrations in the quenched melt (glass) were not determined in previous studies and the effect of H_2O remains to be established quantitatively.

The major difference between this work and previous inverse experimental studies on arc basalts is that experimental conditions more relevant to arc settings were imposed, i.e., presence of water and oxidized fO_2. To satisfy these requirements, several aspects of the high pressure methodology were adapted, as detailed below.

3.2. Starting Materials and Capsules

Sample STV 301 (MgO = 12.5 wt.%, Heath et al., 1998) was selected for the experimental study. It has Ni = 250 ppm and Cr = 728 ppm (Table 1), contains olivine, clinopyroxene and spinel microphenocrysts, and has an olivine/whole-rock Kd(Fe-Mg) = 0.33 (Heath et al., 1998), indicating no significant crystal accumulation. Two types of glasses with different initial H_2O contents were used as starting materials. First, a nominally dry glass was prepared by fusing 8 g of the powdered rock sample in air at 1400°C for several hours (Macdonald et al., 1998). Second, a hydrous glass was synthesized by reacting the previous glass plus ~ 2.6 wt.% H_2O at 1500°C, 15 kbar, for 1 h. Three batches of hydrous glasses were used in this study. The water concentration of the starting glasses was analyzed by Karl-Fischer titration (Behrens et al., 1996) with an uncertainty of ± 0.1 wt.%. The glass prepared at 1 atm contains 0.10 wt.% H_2O and has a Fe^{3+}/Fe^{2+} ratio (at.) of 4.88 (Table 1) as determined by Mössbauer spectroscopy. The hydrous glasses have final H_2O concentrations (2.84 to 2.91 wt.%) slightly higher than the amount of water initially present in the capsule, which suggests that they gained some H_2O during synthesis. Because the hydrous glasses were available in small quantities, no Mössbauer analysis was performed. Some starting glasses were examined by FTIR to check for the presence of H_2O and absence of C-bearing species.

About 10 mg of glass (either nominally dry or hydrous) was loaded into a $Au_{70}Pd_{30}$ capsule (length: 6 to 8 mm, ID: 2.6 mm, wall thickness: 0.2 mm) which was welded shut with a small torch and then placed in the furnace assembly. The choice of $Au_{70}Pd_{30}$ capsules was dictated by the necessity to impose oxidizing conditions (i.e., above graphite stability) and to limit the presence of C as an additional component, therefore eliminating graphite containers. It is shown below that the performances of $Au_{70}Pd_{30}$ alloy with respect to Fe loss are reasonably good in the experimental T-fO_2 range covered in this study (i.e.,

Table 2. Conditions and Results for Experiments with the Dry Starting Glass.

Run#	P (kbar)	T (°C)	Duration (hour)	Results	H_2O glass (wt%)	ΔNNO▪	Σr²*	ΔFeO§ (%)
15	7.5	1200	19.25	gl(97)‡, ol(2), sp(1)	1.76°	+2.1	0.59	−7.4
16	8	1220	16.75	gl(97), ol(2), sp(1)	1.0	+1.7	2.52	−15.8
29	9	1220	18	gl(99), ol(tr), sp(1)	1.3	+0.9	2.18	−15.4
32	9	1200	18	gl(99), ol(tr), sp(1)	1.8	+1.0	2.28	−15.7
11	10	1240	16.75	gl(100)	0.77°	—	—	−7.4
17	10.5	1230	17.5	gl(97), ol(2), sp(1)	1.26°	+1.2	2.76	−17.1
10	10	1220	23.25	gl(87), ol(10), opx(−9) cpx(14), sp(tr)	1.5	+1.4	1.56	−12.4
9	10.5	1200	14.5	gl(90), ol(5) cpx(5), sp(tr)	0.9	+2.6	0.03	−1.6
30	11	1220	17.5	gl(89), ol(4) cpx(6), sp(1)	1.9	+1.2	0.47	−7.0
19	12	1240	17	gl(100)	1.07°	—	—	−5.5
39	12	1260 →1220	2 →18	gl(53), opx(7) cpx(35), sp(5)	1.9	+0.6	0.16	−3.5
35	12	1200	19	gl(85), ol(4) cpx(11), sp?	1.4	—	3.78	−20.4
8	13	1250	21.25	gl(100)	1.77°	—	—	−27.4
20	12.5	1210	18	gl(58), opx(6) cpx(32), sp(4)	1.7	+1.8	0.01	−0.3
23	13	1230	13	gl(77), opx(2) cpx(19), sp(2)	0.9	+0.9	1.05	−10.5
21	14.5	1280	18	gl(100)	1.56°	—	—	−26.4
25	15	1260	12	gl(74), opx(3) cpx(22), sp(1)	1.1	+1.0	0.08	−2.8
24	15	1240	12.5	gl(77), opx(3) cpx(20)	1.6	—	1.55	−11.8
26	17.5	1240	16	gl(54), opx(5) cpx(41)	2.3	—	2.42	−13.6
28	18	1290	12	gl(100)	0.87°	—	—	−21.0

‡ Phase proportions calculated by mass balance.

° H_2O concentration by ion microprobe; other H_2O concentration data are estimated with the by difference method.

▪ ΔNNO = $\log fO_2$ - $\log fO_2$ of the NNO buffer calculated at P and T (Chou, 1987). Experimental fO_2 calculated from olivine-spinel equilibria (Ballhaus et al., 1991). For olivine-free but spinel-bearing charges, experimental fO_2 calculated from spinel-liquid equilibria (Maurel and Maurel, 1982; Danyushevsky and Sobolev, 1996; Kress and Carmichael, 1991). See also text.

* Sum of residuals for the mass balance calculations.

§ ΔFeO is apparent loss or gain of FeO calculated as (wt%) 100* (FeO_{calc}–$FeO_{starting\ glass}$)/$FeO_{starting\ glass}$. For crystal-bearing charges, FeO_{calc} is concentration of FeO (total Fe as FeO) in the charge calculated by mass balance. For crystal-free charges, FeO_{calc} is concentration of FeO (total Fe as FeO) in the glass measured by electron microprobe.

gl: glass, ol: olivine, opx: low-Ca pyroxene, cpx: high-Ca pyroxene, sp: spinel, tr: a trace of.

ΔNNO > 0 and T < 1300°C), in agreement with previous results (Kawamoto and Hirose, 1994).

3.3. Equipment and Run Procedure

The high-pressure experiments were performed in three end-loaded, 1/2″ piston-cylinder apparatuses at the Geophysical Laboratory, Washington DC, using the hot piston-out technique. The furnace assemblies consisted of graphite tube furnaces, AlSiMag inner parts, and outer sleeves of pyrex and talc imposing a H-rich environment in the high-pressure cell. In all experiments, the $Au_{70}Pd_{30}$ capsule was encased in a 0.8 mm thick AlSiMag sleeve that served as a sample holder. Temperatures were monitored using Pt-Pt_{90}/Rh_{10} thermocouples and are known to better than ± 10°C. After the experiments, checks were made of the position of the thermocouple which needed to be ≤ 1 mm from the top of the capsule. No pressure correction was applied to the thermocouple readings. Reported pressures incorporate calibrations performed using standard mineral reactions (quartz ⇋ coesite and calcite ⇋ aragonite). The pressure uncertainty is ± 1 kbar. Run durations ranged between 10 to nearly 24 h, and were around 16 h on average. The samples were quenched in a few seconds by switching off the power to the furnace.

3.4. Analytical Techniques

Experimental capsules were sectioned, then mounted in epoxy and polished. Phase assemblages were identified by optical and Raman microscopy. Seventeen charges (out of a total of 32) were examined with scanning electron microscopy (SEM).

Electron microprobe analysis of the experimental charges was performed with the Cameca SX 50 of the Service Commun BRGM-CNRS at Orléans, with an acceleration voltage of 15 kV and a counting time of 10 s on peak. Silicate minerals were used as standards. A sample current of 6 nA and beam sizes of 1 to 2 μm were employed for mineral phases and 10 μm for glasses. Analysis of the starting glasses revealed no detectable migration of alkalies under the beam (Table 1) and no correction was applied to the Na_2O and K_2O concentrations (e.g., Pichavant, 1987). Analytical errors are: 2% (SiO_2, Al_2O_3, CaO), 3% (FeO, MgO, TiO_2), 5% (MnO, Na_2O, K_2O) relative. Mass-balance calculations (Albarède, 1995) were performed on all major oxides except MnO and H_2O to estimate the proportions of phases coexisting in a given charge and to evaluate quantitatively the extent of Fe loss (Tables 2, 3).

The H_2O concentrations in glasses were measured with the Cameca IMS-3F ion microprobe of the CRPG, Nancy, using the procedures of Deloule et al. (1995). A negative primary oxygen beam with an intensity of 10 nA was focused to produce a spot of 30 μm diameter. The mass resolution was set to 800. ^1H, ^{28}Si and ^{30}Si were measured; possible interferences or instrumental biases were monitored by checking the Si isotope ratio. An energy offset of −80 eV was applied (Deloule et al., 1995). Counting times varied between 5 s (^1H, ^{30}Si) to 2 s (^{28}Si). Measurement cycles were accumulated for 10 to 20 min on each spot. Between 5 to 8 spots were analysed for each sample. Standards were the starting glasses analyzed by Karl-Fischer titration, thus virtually eliminating matrix effects. The uncertainty on the determined H_2O content is better than 10% relative.

For charges that could not be analyzed for H_2O due to the limited size of their glass pools or access limitations to the ion microprobe, the H_2O contents were estimated using a "by-difference" method modified after Devine et al. (1995). The difference to 100% of electron microprobe analyses was calibrated against the dissolved glass H_2O content, the starting glasses being used as standards. These standard glasses were analyzed together with the experimental glasses during each electron microprobe session. Differences in Fe^{3+}/Fe^{2+} between exper-

Table 3. Conditions and Results for Experiments with the Hydrous Starting Glass.

Run#	P (kbar)	T (°C)	Duration (hour)	Results	H_2O glass (wt%)	ΔNNO▪	Σr^2*	ΔFeO§ (%)
13	9.5	1180	16.25	gl(98)‡, ol(2), sp(tr)	3.71°	+2.5	0.66	−7.5
16	10	1160	17.5	gl(96), ol(3), sp(1)	4.80°	+2.4	0.52	−5.2
6	12.5	1200	17.5	gl(100)	3.51°	—	—	−2.0
9	15	1200	23	gl(100)	4.64°	—	—	−8.9
12	14.5	1180	19	gl(97), ol(2), sp(1)	4.95°	+1.9	0.37	−5.0
11	15	1160	18	gl(70), opx(5) cpx(23), sp(2)	5.8	+2.8	0.15	−3.5
26	15	1220	2	gl(100)	4.77°	—	—	−17.1
		→1180	→18					
17	17.5	1180	12	gl(75), opx(5) cpx(20)	5.3	—	2.59	−17.2
19	17.5	1200	12	gl(75), opx(4) cpx(20), sp(1)	5.2	+1.9	0.38	−5.0
7	19	1250	10.5	gl(100)	3.28°	—	—	−5.5
18	20	1220	12	gl(100)	3.23°	—	—	−5.7
8	19	1200	19.25	gl(98), opx(1) cpx(1)	3.76°	—	2.56	−16.6

‡ Phase proportions calculated by mass balance.

° H_2O concentration by ion microprobe; other H_2O concentration data are estimated with the by difference method.

▪ ΔNNO = $\log fO_2$ - $\log fO_2$ of the NNO buffer calculated at P and T (Chou, 1987). Experimental fO_2 calculated from olivine-spinel equilibria (Ballhaus et al., 1991). For olivine-free but spinel-bearing charges, experimental fO_2 calculated from spinel-liquid equilibria (Maurel and Maurel, 1982; Danyushevsky and Sobolev, 1996; Kress and Carmichael, 1991). See also text.

* Sum of residuals for the mass balance calculations.

§ ΔFeO is apparent loss or gain of FeO calculated as (wt%) 100* (FeO_{calc}–$FeO_{starting\ glass}$)/$FeO_{starting\ glass}$. For crystal-bearing charges, FeO_{calc} is concentration of FeO (total Fe as FeO) in the charge calculated by mass balance. For crystal-free charges, FeO_{calc} is concentration of FeO (total Fe as FeO) in the glass measured by electron microprobe.

gl: glass, ol: olivine, opx: low-Ca pyroxene, cpx: high-Ca pyroxene, sp: spinel, tr: a trace of.

imental and standard glasses were taken into account in the calibration. The error on the estimation of H_2O content with our "by-difference" method is 25% relative for glasses with ~ 4 to 5 wt.% H_2O, increasing up to 100% relative for glasses with ≤ 1 wt.% H_2O.

4. RESULTS

A total of 32 high-pressure near-liquidus experiments were performed, 20 with the nominally dry starting glass and 12 with the hydrous starting glass, in the range 1160 to 1290°C and 7.5 to 20 kbar. Experimental conditions and results are summarized in Tables 2 and 3. Most experiments approached their final (target) temperature from below but 2 experiments were two-stage runs in which the charge was initially kept above the liquidus for 2 h before being isobarically cooled to their final (target) temperature.

4.1. Control of the Melt H_2O Content

In this study, no attempt was made to buffer the H_2O concentration of experimental melts. Rather, the H_2O concentration of the melt in each series was controlled by the composition of the starting glasses (H_2O content and Fe^{3+}/Fe^{2+}) and by the intrinsic properties of the talc-bearing high-pressure assemblies which promoted a H-rich environment around the capsules. Experiments performed with the nominally dry starting product have glass H_2O concentrations ranging between 0.9 and 2.3 wt.% (Table 2), 1.4 ± 0.4 wt.% on average. Glasses from experiments performed with the hydrous starting material have H_2O concentrations ranging between 3.3 and 5.8 wt.% (Table 3), 4.4 ± 0.9 wt.% on average. In the following, experiments performed with the nominally dry starting glass will be designated as the 1.5 wt.% H_2O experiments and those with the hydrous starting glass as the 4.5 wt.% H_2O experiments. The dispersion of H_2O concentrations between charges is, respectively, 29 and 20% relative for the 1.5 wt.% and 4.5 wt.% H_2O series of experiments. Several factors contribute to this dispersion, including variations in the proportion of crystals from one charge to the other and, to a lesser extent, differences in Fe loss among charges (see below). Part of the dispersion in H_2O concentrations is also analytical. The sensitivity of the "by-difference" method is poor for concentrations < 2 wt.% H_2O. For the 4.5 wt.% H_2O series of experiments, the ion microprobe data and the "by-difference" estimates are within 0.14 wt.% H_2O from each other on average (9 charges), but the deviation increases up to 0.65 wt.% H_2O for the 1.5 wt.% H_2O series of experiments (7 charges).

The data on H_2O content imply that all charges gained some H_2O during the experiments. As noted above, the first series of experiments (Table 2) was performed from an almost dry starting material (Table 1). Yet, glasses from this series have average H_2O concentrations of 1.4 wt.%, indicating an average gain of 1.3 wt.% H_2O. This is very close to the average gain of H_2O which can be calculated for the 4.5 wt.% H_2O series of glasses (i.e., ~ 1.5 wt.%), suggesting that the mechanism responsible for capsules gaining H_2O is the same whatever the glass starting material used (Table 1). Gain of H_2O in piston-cylinder experiments is commonly explained by the oxidation of hydrogen diffusing through the capsule walls, in relation to the reduction of an oxidized component of the charge such as Fe_2O_3 (e.g., Eggler et al., 1974; Brooker et al., 1998). The use of strongly oxidized glass starting materials in combination with talc-bearing assemblies as in this study would promote such a mechanism. However, calculations of the amount of H_2O generated (assuming an initial glass Fe^{3+}/Fe^{2+} ratio as in Table 1 and a final glass Fe^{3+}/Fe^{2+} ratio of 0.4, as determined below) yields a maximum of 0.62 wt.% H_2O, i.e., substantially less than the monitored increase in H_2O concentration (1.3 to 1.5 wt.%), which underlines the need for an additional H_2O supply mechanism. Although reduction of Fe^{3+} and Fe^{2+} to

metallic Fe by alloying with the $Au_{70}Pd_{30}$ capsule could generate more H_2O, no correlation exists between the H_2O concentration and the relative Fe loss (Tables 2, 3). Therefore, direct infiltration of H_2O from the high-pressure assembly to the charge across the $Au_{70}Pd_{30}$ capsule is thought to be the main additional H_2O supply mechanism. Recent studies have documented the possibility of O and H_2O migration through noble metal capsules at high temperatures in piston-cylinder studies (Patiño-Douce and Beard, 1994; Tuckenbrodt et al., 1997). Therefore, it is likely that not only H_2, but also H_2O, were supplied to the charge by the talc-bearing high-pressure cells used in this study.

4.2. Control of fO_2

No attempt was made to buffer the fO_2 of the experimental charges by using, for example, double capsules with conventional oxygen buffers. This is because at high temperatures these buffers cannot last for sufficiently long durations if the fH_2 imposed by the high-pressure cell is in strong contrast to that of the buffer (e.g., Scaillet et al., 1992). Rather, the fO_2 in this study was controlled by the initial Fe^{3+}/Fe^{2+} ratios of the starting glasses and by the fH_2 (and fH_2O) imposed by the high-pressure cells. For charges crystallizing olivine and spinel at equilibrium, experimental fO_2 was calculated from the formulation of Ballhaus et al. (1991). For charges lacking olivine but crystallizing spinel, experimental fO_2 were calculated from melt Fe^{3+}/Fe^{2+} ratios (Kress and Carmichael, 1991), assuming that the melt iron redox equilibrium is not affected by the presence of H_2O (Carmichael, 1991). Melt Fe^{3+}/Fe^{2+} ratios were obtained from the composition of Cr-Al spinels crystallizing in experimental products (Maurel and Maurel, 1982; Danyuschevsky and Sobolev, 1996). Because the data of Maurel and Maurel (1982) are for dry basaltic melts at 1 atm, the effects of H_2O and pressure on Fe^{3+}/Fe^{2+} partitioning between spinel and melt are unknown and have been assumed to be negligible (see Danyuschevsky and Sobolev, 1996). ΔNNO (difference in log fO_2 from that of the nickel-nickel oxide buffer, NNO) values obtained from Ballhaus et al. (1991) are higher by 0.2 log units on average than those calculated with the spinel-melt method on the same charges. As an additional check, the spinel-melt method was tested on the hydrous lherzolite partial melting experiments of Hirose and Kawamoto (1995) and yielded fO_2 lower by 0.2 log unit on average than the calculations of those authors. Thus, the spinel-melt is a reliable method of calculation of fO_2 for our olivine-free charges.

All fO_2 data in Tables 2 and 3 are referenced to the NNO buffer calculated at the P and T of the experiment (Chou, 1987). The ΔNNO values range between + 0.6 to + 2.6 (+ 1.4 $\pm$ 0.6 on average, Table 2) in the 1.5 wt.% H_2O series of experiments and between + 1.9 to + 2.8 (+ 2.3 $\pm$ 0.4 on average, Table 3) in the 4.5 wt.% H_2O series of experiments. Therefore, all experiments from this study were equilibrated under relatively oxidizing conditions, although, on average, the 4.5 wt.% H_2O experiments are more oxidized than the 1.5 wt.% H_2O (Fig. 4).

Melt Fe^{3+}/Fe^{2+} ratios were obtained directly from spinel composition (Maurel and Maurel, 1982; Danyuschevsky and Sobolev, 1996) or indirectly, from fO_2 data, by using the empirical expression of Kress and Carmichael (1991). The Fe^{3+}/Fe^{2+} derived by this method are of $\sim$ 0.4 and $\sim$ 0.5, respectively, for the 1.5 and 4.5 wt.% H_2O series of experiments. For charges lacking spinel and whose fO_2 is unknown, melt Fe^{3+}/Fe^{2+} ratios were calculated from Kress and Carmichael (1991), taking the average fO_2 for each series of experiments. By comparison with the Fe^{3+}/Fe^{2+} ratio of the starting glass (4.88, Table 1), the Fe^{3+}/Fe^{2+} ratios thus obtained indicate that reduction of Fe^{3+} occurred during the experiments. However, it is important to point out that a substantial fraction of iron exists as Fe^{3+} in basaltic melts from this study. Melt FeO (and not FeO_t) concentrations are used below to calculate the Fe-Mg mineral-melt partition coefficients.

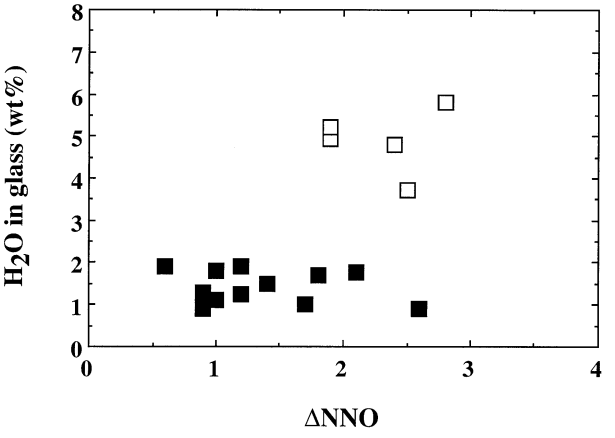

Fig. 4. H_2O content of experimental glasses from this study plotted as a function of fO_2, expressed as deviation from the NNO buffer (ΔNNO). (■): experiments performed with the dry starting glass (Table 2); (□): experiments performed with the hydrous starting glass (Table 3).

4.3. Evaluation of Fe Loss

The importance of Fe-loss was evaluated for charges above the liquidus from glass compositions and for charges below the liquidus from mass-balance calculations (Tables 2, 3). Fe-loss is mostly a function of temperature. Below 1200°C, Fe-loss is of a few % (relative of the total FeO present), except for three runs (#26, 17 and 8, Table 3). Above 1250°C, Fe-loss may be more severe, although exceptions exist (#25, Table 2, #7, Table 3). Seventeen runs out of the 32 reported experienced Fe losses $\leq$ 10% relative, 4 (all from the 1.5 wt.% H_2O experiments) had $>$ 20% loss (Table 2) and none had more than 28% loss. These results show that Fe-loss has been minimized in this study. They confirm the relatively good performances of $Au_{70}Pd_{30}$ capsules with respect to Fe-loss under oxidizing conditions (Kawamoto and Hirose, 1994), at least below 1200°C. However, Fe-loss has not been totally suppressed.

4.4. Approach to Equilibrium and Quench Crystallization

In this study, we have avoided the use of crystalline starting materials because melting experiments involve notoriously sluggish reactions and, as a rule, are more difficult to equilibrate than crystallization experiments (e.g., Green, 1976; Gust

and Perfit, 1987; Bartels et al., 1991; Draper and Johnston, 1992; Scaillet et al., 1995; Scaillet and Evans, 1999; Martel et al., 1999). Attainment of equilibrium cannot be documented from reversals, therefore, because all experiments from this study are of crystallization type. Nevertheless, several lines of evidence can be used to evaluate the approach to equilibrium. These are the following:

1. Experimental durations (16 h on average) were relatively long compared to other studies of this type (Tatsumi, 1982; Tatsumi et al., 1983; Gust and Perfit, 1987; Kushiro, 1987; Baker et al., 1994; Tatsumi et al., 1994). Bartels et al. (1991) found that 6 h were sufficient to obtain reproducible phase assemblages and proportions in near-liquidus anhydrous experiments on a partially crystalline high alumina basalt at 1280°C, 12 kbar. Because reaction kinetics are likely to be faster in presence of H_2O, experimental durations in this study were such that equilibrium should have been closely approached.
2. To test the reactivity of our glass starting materials and check for reproducibility, 2 two-stage runs (one for each series of melt H_2O concentrations) were performed. Experiments were first kept at superliquidus conditions for 2 h. Temperatures were then dropped isobarically and maintained for 18 h (Tables 2, 3). Results from these two-stage runs agreed with those from the other experiments within uncertainties (Fig. 5), which supports the conclusion that our results are reproducible and independent of how experimental temperatures are approached.
3. In a given charge, mineral phases and glass have homogeneous compositions. This is best documented by examining the standard deviations of the electron microprobe analyses (Tables 4, 5), which are in the same range as the analytical dispersion. The only exception is spinel which is slightly heterogeneous in some of the 1.5 wt.% H_2O charges, as revealed by standard deviations $>$ 1 wt.% for Cr_2O_3, Al_2O_3 and FeO_{tot} (Table 4).
4. Mineral-melt Kd calculated from the experimental data are in agreement with results from the literature under comparable P-T conditions (see below for details) and suggest a close approach to chemical equilibrium.
5. Results of the mass-balance calculations are detailed on Tables 2 and 3. All charges but one (#10, Table 2) could be successfully mass-balanced. However, sums of residuals of the mass-balance calculations vary widely, from 0.01 to $>$ 3 and strongly correlate with Fe loss (Tables 2, 3). Charges with Fe losses $<$ 10% relative have $\Sigma R^2 < 1$ (0.31 on average), which compares favourably with residuals from other studies (e.g., 0.02 to 0.13, Gaetani and Grove, 1998; 0.2, Falloon and Danyushevsky, 2000), and demonstrate that a constant bulk silicate composition was maintained. In contrast, those with Fe losses $>$ 10% relative are characterized by $\Sigma R^2 > 1$, thus indicating deviation from a constant bulk silicate composition. Charge #10 has a calculated negative proportion of opx (Table 2), suggesting that an equilibrium phase assemblage was not obtained. Because this charge is the only one containing the 4-phase assemblage ol + cpx + opx + sp, it has been kept in Table 2 but is neither plotted on, nor taken into account in the construction of, the phase diagram (Fig. 5).

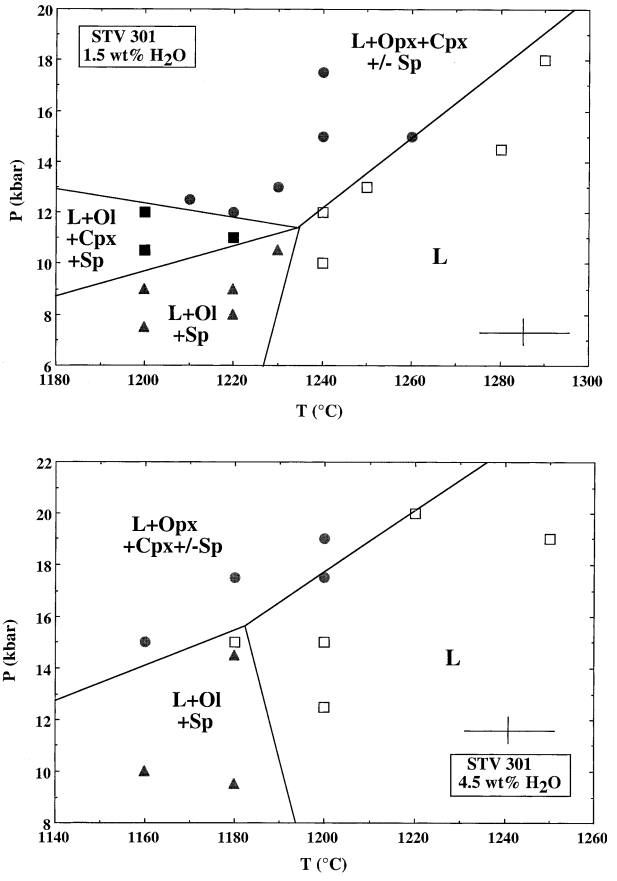

Fig. 5. Near-liquidus phase relations for STV301 with 1.5 wt.% H_2O (top) and 4.5 wt.% H_2O in the melt (bottom). Symbols: (▲) L + Ol + Sp; (●) L + Opx + Cpx +/- Sp; (■) L + Ol + Cpx + Sp; (□) L (above liquidus). Abbreviations: Ol: olivine, Opx: orthopyroxene; Cpx: clinopyroxene; Sp: Cr-Al spinel; L: glass. The cross shown in both diagrams represents the experimental uncertainty. The slightly negative slope of the low pressure liquidus for the 4.5 wt.% H_2O diagram is also constrained by additional experiments at 4 kbar (Macdonald et al., 1998; in preparation) that have determined a liquidus temperature of 1200°C for STV301 with ~ 4.5 wt.% H_2O in the melt.

6. The crystalline phases obtained in this study are euhedral and have homogeneous sizes, up to 100 μm for olivine, in the 10 to 30 μm range for orthopyroxene, 10 μm for clinopyroxene and $<$ 10 μm for spinel. The presence of quench crystals is common in the 4.5 wt.% H_2O series of experiments. The proportion of materials crystallized during the quench is variable, but never important enough to prevent large glass pools being preserved for analysis. The ΣR^2 values (Table 3) indicate that the amount of quench crystals is never high enough to affect the mass-balance calculations.

To summarize, we believe that the experimental data presented here closely approach equilibrium phase assemblages and compositions. The main problem is the presence of some dispersion in bulk silicate composition (and H_2O content, see above) between charges. Nevertheless, it should be emphasized that this dispersion is never large enough to affect the phase equilibria. For example, results from run #35 (Fe loss of 20.4% relative) are consistent (see Fig. 5) with run #9 and #20 (both with relative Fe losses $<$ 5%, Table 2).

Table 4. Compositions of phases in the the 1.5 wt% H_2O series of experiments.

Run#	Phase	SiO_2	TiO_2	Al_2O_3	Cr_2O_3	FeO_{tot}	MnO	MgO	CaO	Na_2O	K_2O	total	
15	gl*(4)§	48.28 (26)†	1.04 (5)	16.17 (21)	0.03 (4)	8.42 (49)	0.26 (10)	11.41 (11)	11.58 (14)	2.33 (6)	0.47 (6)	98.76	Mg#79.1°
	ol(2)	41.47 (5)	0.03 (3)	0.04 (2)	0.10 (2)	7.42 (26)	0.21 (5)	50.67 (39)	0.28 (3)	0.02 (2)	0.00 (0)	100.24	Fo92.4
	sp(6)	0.49 (33)	0.43 (7)	38.92 (83)	17.73 (76)	21.93 (48)	0.17 (13)	19.13 (25)	0.19 (9)	0.03 (2)	0.03 (2)	99.05	Cr#23.4
16	gl(4)	48.52 (11)	1.14 (7)	16.11 (15)	0.05 (6)	7.56 (38)	0.20 (14)	11.79 (9)	11.80 (23)	2.33 (14)	0.50 (4)	97.90	Mg#80.1
	ol(4)	41.16 (39)	0.02 (2)	0.23 (10)	0.06 (4)	7.52 (23)	0.16 (4)	50.25 (19)	0.28 (6)	0.03 (3)	0.01 (1)	99.72	Fo92.4
	sp(6)	0.26 (10)	0.86 (28)	38.80 (176)	20.05 (149)	18.74 (261)	0.07 (9)	19.40 (38)	0.12 (4)	0.02 (3)	0.02 (2)	98.34	Cr#25.7
29	gl(4)	48.49 (10)	1.13 (5)	15.87 (26)	0.03 (5)	7.71 (33)	0.14 (10)	12.30 (48)	11.41 (12)	2.36 (8)	0.50 (6)	97.69	Mg#78.7
	ol(2)	40.91 (39)	0.00 (0)	0.11 (13)	0.00 (0)	7.24 (9)	0.08 (11)	50.14 (11)	0.26 (1)	0.01 (1)	0.02 (2)	98.77	Fo92.4
	sp(1)	0.21	0.44	42.76	20.71	14.64	0.15	19.97	0.15	0.01	0.03	99.07	Cr#24.5
32	gl(4)	48.66 (43)	1.10 (4)	15.68 (12)	0.06 (10)	7.63 (26)	0.18 (7)	12.37 (9)	11.38 (22)	2.42 (9)	0.53 (2)	97.14	Mg#79.3
	ol(3)	41.29 (21)	0.01 (1)	0.10 (1)	0.09 (8)	7.34 (34)	0.16 (3)	49.93 (50)	0.34 (7)	0.02 (2)	0.02 (1)	99.30	Fo92.4
	sp(2)	0.62 (62)	0.28 (5)	43.99 (31)	18.22 (76)	15.32 (45)	0.19 (6)	19.82 (6)	0.23 (27)	0.01 (1)	0.04 (1)	98.72	Cr#21.7
11	gl(4)	48.03 (40)	1.16 (3)	15.50 (9)	0.14 (11)	8.45 (4)	0.18 (18)	12.43 (13)	11.31 (21)	2.29 (13)	0.51 (4)	97.92	Mg#78.5
17	gl(4)	48.57 (43)	1.15 (6)	16.21 (21)	0.12 (9)	7.52 (8)	0.17 (10)	11.78 (26)	11.62 (38)	2.37 (11)	0.51 (3)	98.67	Mg#78.9
	ol(3)	41.94 (49)	0.01 (1)	0.11 (3)	0.07 (8)	7.77 (42)	0.26 (4)	50.06 (49)	0.31 (6)	0.02 (2)	0.00 (0)	100.55	Fo91.8
	sp(6)	0.18 (5)	0.49 (13)	41.74 (173)	20.26 (191)	16.94 (139)	0.18 (15)	19.96 (42)	0.12 (3)	0.05 (7)	0.01 (2)	99.93	Cr#24.6
10	gl(4)	48.76 (12)	1.32 (5)	18.05 (29)	0.02 (2)	8.02 (27)	0.19 (10)	9.45 (23)	10.57 (13)	2.97 (18)	0.65 (5)	97.46	Mg#74.2
	ol(3)	40.85 (53)	0.03 (1)	0.07 (2)	0.12 (4)	10.26 (39)	0.26 (7)	48.22 (98)	0.20 (4)	0.02 (3)	0.00 (0)	100.03	Fo89.4
	opx(2)	51.33 (13)	0.25 (10)	8.00 (11)	0.10 (9)	8.27 (16)	0.18 (1)	28.83 (71)	2.35 (18)	0.06 (1)	0.00 (0)	99.37	En83.5Wo4.9
	cpx(3)	49.54 (36)	0.53 (6)	8.31 (38)	0.08 (12)	6.56 (10)	0.17 (5)	17.26 (44)	17.38 (71)	0.71 (3)	0.01 (1)	100.55	En53.4Wo39.1
	sp▪(1)	0.37	0.28	51.51	8.35	17.94	0.11	20.11	0.13	0.00	0.01	98.81	Cr#9.8
9	gl (4)	48.28 (57)	1.18 (6)	16.88 (39)	0.04 (3)	9.05 (33)	0.19 (12)	9.75 (8)	11.55 (14)	2.50 (14)	0.57 (1)	97.93	Mg#75.9
	ol(5)	40.40 (55)	0.01 (2)	0.12 (5)	0.04 (6)	8.09 (25)	0.29 (10)	49.33 (37)	0.26 (7)	0.02 (2)	0.01 (2)	98.57	Fo91.5
	cpx(7)	47.55 (82)	0.55 (14)	8.30 (131)	0.26 (12)	6.85 (72)	0.12 (13)	16.56 (69)	17.36 (94)	0.55 (8)	0.06 (7)	98.16	En52.0Wo39.5
	sp(5)	0.26 (12)	0.44 (6)	35.96 (149)	13.65 (107)	27.91 (68)	0.16 (13)	17.90 (48)	0.24 (4)	0.01 (1)	0.03 (3)	96.56	Cr#20.3
30	gl(4)	48.57 (24)	1.20 (5)	16.65 (14)	0.07 (8)	8.60 (15)	0.12 (11)	10.41 (7)	11.28 (17)	2.58 (4)	0.53 (1)	97.06	Mg#74.2
	ol(3)	40.85 (27)	0.00 (0)	0.12 (2)	0.03 (5)	8.85 (5)	0.13 (15)	49.05 (9)	0.20 (9)	0.00 (0)	0.02 (2)	99.25	Fo90.9
	cpx(4)	49.04 (39)	0.40 (16)	7.96 (36)	0.33 (9)	5.74 (28)	0.06 (8)	17.35 (9)	16.99 (41)	0.59 (8)	0.01 (2)	98.47	En54.2Wo37.9
	sp(4)	0.97 (49)	0.29 (8)	49.16 (49)	9.69 (121)	17.77 (27)	0.15 (7)	19.95 (15)	0.38 (14)	0.04 (2)	0.02 (2)	98.42	Cr#11.7
19	gl(4)	48.19 (25)	1.15 (9)	15.41 (21)	0.12 (9)	8.62 (17)	0.18 (14)	12.28 (32)	11.20 (16)	2.33 (18)	0.51 (4)	99.00	Mg#78.1
39	gl(5)	50.07 (46)	1.55 (7)	18.84 (22)	0.03 (5)	8.03 (11)	0.19 (16)	7.51 (6)	9.21 (21)	3.70 (12)	0.88 (4)	97.08	Mg#67.5
	opx(7)	51.21 (72)	0.27 (8)	8.17 (75)	0.12 (7)	8.79 (92)	0.17 (11)	27.99 (56)	2.14 (54)	0.10 (4)	0.00 (0)	98.96	En81.8Wo4.4
	cpx(5)	48.72 (54)	0.59 (7)	8.97 (29)	0.07 (7)	6.87 (38)	0.22 (7)	15.56 (35)	17.27 (52)	0.72 (9)	0.01 (1)	99.00	En49.7Wo39.3
	sp(5)	0.15 (5)	0.76 (16)	35.85 (203)	19.03 (63)	27.02 (219)	0.25 (7)	14.75 (68)	0.20 (5)	0.01 (1)	0.02 (3)	97.79	Cr#26.3
35	gl(4)	48.97 (31)	1.18 (8)	17.71 (32)	0.06 (6)	7.49 (12)	0.19 (7)	10.32 (7)	10.70 (23)	2.76 (8)	0.63 (8)	97.59	Mg#77.1
	ol(3)	41.05 (46)	0.00 (0)	0.09 (1)	0.04 (4)	9.70 (63)	0.10 (6)	48.66 (35)	0.19 (6)	0.01 (2)	0.02 (1)	99.86	Fo89.9
	cpx(3)	49.81 (31)	0.58 (6)	8.14 (42)	0.31 (18)	5.88 (17)	0.19 (14)	17.79 (52)	16.22 (89)	0.59 (13)	0.03 (2)	99.54	En55.4Wo36.0
8	gl(4)	49.09 (41)	1.10 (4)	15.85 (19)	0.02 (8)	6.62 (37)	0.14 (10)	12.74 (43)	11.44 (18)	2.47 (21)	0.52 (4)	97.98	Mg#82.7
20	gl(2)	49.80 (33)	1.33 (3)	18.55 (19)	0.00 (0)	8.48 (25)	0.19 (7)	7.98 (20)	9.37 (6)	3.52 (17)	0.79 (1)	97.15	Mg#70.4
	opx(1)	50.49	0.28	9.05	0.03	9.38	0.08	28.82	1.69	0.16	0.00	99.98	En83.9Wo3.3
	cpx(1)	48.78	0.62	8.68	0.13	7.37	0.13	15.80	17.54	0.80	0.02	99.87	En50.3Wo39.9
	sp(4)	0.20 (17)	0.67 (7)	33.32 (156)	19.35 (150)	27.85 (17)	0.18 (12)	15.91 (39)	0.12 (5)	0.01 (1)	0.05 (3)	97.66	Cr#28.1
23	gl(4)	48.25 (33)	1.36 (11)	17.51 (14)	0.02 (3)	8.56 (12)	0.12 (8)	10.16 (16)	10.44 (18)	2.92 (17)	0.66 (5)	98.13	Mg#72.9
	opx(2)	52.65 (38)	0.17 (6)	8.09 (69)	0.23 (8)	7.18 (35)	0.20 (7)	29.73 (1)	2.32 (21)	0.12 (3)	0.00 (0)	100.69	En84.2Wo4.9
	cpx(2)	50.09 (8)	0.40 (9)	8.15 (13)	0.38 (4)	5.82 (35)	0.21 (11)	18.31 (17)	16.42 (9)	0.68 (4)	0.00 (0)	100.46	En56.2Wo36.4
	sp(7)	0.29 (9)	0.34 (5)	41.77 (153)	18.83 (177)	18.58 (82)	0.13 (11)	18.82 (33)	0.20 (9)	0.00 (0)	0.02 (2)	98.98	Cr#23.2
21	gl(4)	49.40 (26)	1.10 (9)	15.80 (11)	0.04 (6)	6.71 (33)	0.23 (15)	12.38 (12)	11.42 (22)	2.40 (7)	0.52 (3)	98.58	Mg#82.2
25	gl(4)	47.99 (31)	1.39 (7)	17.52 (12)	0.04 (6)	9.30 (52)	0.08 (12)	10.07 (23)	10.11 (12)	2.86 (6)	0.63 (5)	97.87	Mg#70.9
	opx(3)	52.36 (99)	0.18 (6)	7.26 (119)	0.08 (1)	7.80 (12)	0.11 (10)	29.36 (61)	2.05 (3)	0.16 (2)	0.02 (2)	99.38	En84.6Wo4.4
	cpx(2)	48.79 (59)	0.44 (2)	9.30 (43)	0.16 (2)	6.81 (47)	0.14 (4)	16.64 (23)	16.80 (28)	0.94 (8)	0.05 (4)	100.07	En53.8Wo39.1
	sp(4)	0.36 (17)	0.44 (6)	37.83 (97)	20.68 (108)	21.01 (26)	0.28 (6)	17.35 (34)	0.14 (10)	0.03 (4)	0.01 (1)	98.13	Cr#26.8
24	gl(4)	48.28 (43)	1.35 (12)	17.77 (7)	0.07 (6)	8.75 (12)	0.14 (12)	9.91 (23)	10.07 (8)	3.01 (6)	0.65 (3)	97.30	Mg#72.9
	opx(1)	51.07	0.18	9.05	0.21	7.82	0.27	28.88	2.22	0.14	0.00	99.85	En85.3Wo4.5
	cpx(2)	49.61 (83)	0.41 (9)	8.52 (71)	0.20 (13)	5.87 (6)	0.17 (8)	17.27 (81)	15.94 (68)	0.82 (4)	0.02 (3)	98.83	En54.3Wo36.4
26	gl(4)	49.46 (21)	1.67 (7)	18.90 (40)	0.00 (0)	8.51 (22)	0.20 (9)	7.88 (5)	8.68 (17)	3.61 (15)	1.11 (4)	96.63	Mg#68.5
	opx(2)	50.54 (7)	0.20 (1)	10.58 (4)	0.17 (3)	8.86 (25)	0.14 (1)	28.11 (1)	1.59 (1)	0.16 (4)	0.04 (3)	100.31	En82.6Wo3.4
	cpx(3)	48.29 (35)	0.58 (5)	11.01 (6)	0.11 (11)	7.28 (4)	0.10 (3)	15.60 (20)	15.12 (37)	1.18 (14)	0.02 (3)	99.29	En51.8Wo36.0
28	gl(4)	48.67 (32)	1.07 (4)	16.10 (14)	0.12 (9)	7.21 (11)	0.10 (11)	12.51 (28)	11.45 (10)	2.26 (9)	0.49 (4)	97.26	Mg#81.2

* Glass analyses normalized to 100% anhydrous, with all Fe as FeO. Unnormalized total is reported.

§ Number of microprobe analyses.

† One standard deviation in terms of least unit cited.

° Mg# calculated as molar MgO/(MgO+FeO). See text for calculations of FeO. Fo = at Mg/(Mg+Fe). Cr# = at. Cr/(Cr+Al). En = at. Mg/(Mg+Fe+Ca), Wo = at. Ca/(Mg+Fe+Ca) with Fe as Fe^{2+}.

▪ Spinel population with heterogeneous Cr/(Cr+Al).

Abbreviations as in Table 2.

Table 5. Compositions of Phases in the 4.5 wt% H_2O Series of Experiments.

Run#	Phase	SiO_2	TiO_2	Al_2O_3	Cr_2O_3	FeO_{tot}	MnO	MgO	CaO	Na_2O	K_2O	total	
13	gl*(4)[§]	47.89 (35)[†]	1.18 (4)	16.39 (6)	0.06 (2)	8.52 (29)	0.09 (7)	11.61 (22)	11.38 (14)	2.36 (4)	0.52 (5)	95.00	Mg#79.9°
	ol(3)	41.37 (45)	0.00 (0)	0.07 (2)	0.14 (16)	7.60 (20)	0.14 (12)	50.18 (24)	0.23 (4)	0.00 (0)	0.01 (2)	99.74	Fo92.2
	sp(4)	0.30 (18)	0.53 (7)	35.97 (49)	18.34 (53)	24.82 (62)	0.08 (10)	16.41 (17)	0.18 (3)	0.02 (3)	0.01 (1)	96.67	Cr#25.5
16	gl(4)	47.95 (57)	1.16 (3)	16.53 (15)	0.07 (8)	8.47 (10)	0.20 (16)	10.92 (26)	11.79 (41)	2.40 (11)	0.51 (4)	94.58	Mg#78.6
	ol(2)	41.76 (16)	0.00 (0)	0.03 (2)	0.04 (5)	7.40 (12)	0.23 (7)	50.14 (25)	0.21 (1)	0.01 (1)	0.00 (0)	99.82	Fo92.3
	sp(5)	0.28 (20)	0.48 (4)	34.14 (74)	19.52 (10)	24.20 (20)	0.16 (8)	18.17 (60)	0.17 (11)	0.03 (3)	0.01 (1)	97.20	Cr#27.7
6	gl(4)	47.69 (75)	1.13 (3)	15.64 (6)	0.03 (3)	8.95 (53)	0.20 (2)	12.47 (26)	11.18 (22)	2.18 (11)	0.51 (5)	95.42	Mg#79.1
9	gl(4)	48.26 (20)	1.13 (7)	15.79 (16)	0.07 (8)	8.31 (17)	0.12 (5)	12.38 (5)	11.21 (29)	2.21 (6)	0.50 (3)	94.55	Mg#79.9
12	gl(4)	48.52 (22)	1.13 (6)	15.96 (13)	0.03 (3)	8.66 (24)	0.12 (6)	11.60 (22)	11.20 (25)	2.27 (2)	0.51 (6)	94.99	Mg#77.2
	ol(4)	41.65 (21)	0.03 (3)	0.08 (3)	0.01 (2)	7.68 (19)	0.08 (2)	49.90 (37)	0.27 (3)	0.02 (3)	0.01 (2)	99.73	Fo92.1
	sp(3)	0.43 (49)	0.30 (3)	40.69 (48)	17.19 (72)	19.95 (66)	0.11 (0)	19.19 (55)	0.13 (6)	0.03 (5)	0.00 (1)	98.02	Cr#22.1
11	gl(4)	48.81 (48)	1.44 (6)	18.02 (19)	0.01 (2)	9.23 (26)	0.23 (6)	9.50 (9)	9.70 (16)	2.89 (22)	0.82 (6)	92.83	Mg#74.6
	opx(2)	51.69 (11)	0.18 (2)	6.76 (35)	0.19 (13)	7.68 (11)	0.22 (4)	30.25 (11)	1.35 (12)	0.09 (4)	0.00 (0)	98.41	En87.0Wo2.7
	cpx(2)	48.35 (47)	0.53 (9)	7.97 (32)	0.27 (23)	6.39 (1)	0.22 (6)	15.75 (16)	18.75 (31)	0.68 (10)	0.01 (1)	98.92	En49.7Wo42.9
	sp(5)	0.28 (24)	0.36 (6)	49.64 (85)	2.31 (64)	25.41 (39)	0.13 (13)	19.14 (36)	0.16 (7)	0.02 (2)	0.01 (2)	97.46	Cr#3.0
26	gl(5)	48.28 (41)	1.07 (7)	16.47 (24)	0.12 (7)	7.56 (30)	0.17 (7)	12.27 (15)	11.12 (25)	2.43 (6)	0.51 (5)	93.79	Mg#81.3
17	gl(4)	48.01 (26)	1.38 (5)	18.53 (41)	0.04 (7)	8.13 (26)	0.14 (10)	10.24 (7)	9.91 (16)	2.91 (6)	0.70 (2)	93.45	Mg#76.6
	opx(1)	51.55	0.14	7.85	0.18	7.56	0.05	29.83	1.55	0.14	0.00	98.85	En86.3Wo3.3
	cpx(1)	49.08	0.38	8.46	0.43	5.83	0.23	15.88	17.98	0.94	0.06	99.27	En50.9Wo41.5
19	gl(4)	48.06 (27)	1.39 (7)	17.76 (17)	0.07 (6)	9.20 (19)	0.21 (7)	10.32 (30)	9.92 (9)	2.39 (7)	0.67 (1)	93.59	Mg#73.2
	opx(1)	52.04	0.12	8.26	0.00	7.99	0.28	29.84	1.66	0.01	0.01	100.21	En86.1Wo3.3
	cpx(1)	48.74	0.49	8.96	0.31	6.74	0.19	15.59	17.87	0.80	0.00	99.69	En50.3Wo40.9
	sp(1)	0.19	0.28	53.81	3.76	19.37	0.14	20.16	0.16	0.00	0.02	97.87	Cr#4.5
7	gl(4)	47.85 (15)	1.14 (6)	15.78 (11)	0.12 (7)	8.63 (28)	0.14 (10)	12.53 (14)	11.06 (19)	2.24 (12)	0.51 (4)	95.26	Mg#79.5
18	gl(4)	47.75 (23)	1.10 (8)	15.85 (13)	0.07 (7)	8.61 (29)	0.05 (7)	12.38 (20)	11.37 (26)	2.35 (3)	0.47 (2)	95.46	Mg#79.4
8	gl(4)	48.21 (55)	1.14 (7)	16.37 (14)	0.11 (9)	7.72 (8)	0.20 (8)	12.10 (23)	11.25 (13)	2.36 (8)	0.54 (3)	94.51	Mg#80.3
	opx(2)	52.38 (86)	0.10 (4)	8.11 (77)	0.35 (3)	6.70 (35)	0.13 (11)	30.08 (3)	1.73 (8)	0.12 (3)	0.03 (1)	99.73	En86.2Wo3.3
	cpx(2)	48.61 (18)	0.37 (1)	9.96 (43)	0.25 (16)	5.40 (13)	0.12 (4)	15.81 (16)	17.99 (26)	0.97 (7)	0.03 (3)	99.51	En50.9Wo42.0

* Glass analyses normalized to 100% anhydrous, with all Fe as FeO. Unnormalized total is reported.

[§] Number of microprobe analyses.

[†] One standard deviation in terms of least unit cited.

° Mg# calculated as molar MgO/(MgO+FeO). See text for calculations of FeO. Fo = at. Mg/(Mg+Fe). Cr# = at. Cr/(Cr+Al). En = at. Mg/(Mg+Fe+Ca), Wo = at. Ca/(Mg+Fe+Ca) with Fe as Fe^{2+}.

Abbreviations as in Table 2.

4.5. Phase Equilibria

Tables 2 and 3 list phase assemblages and proportions of phases for the two series of experiments. Phase equilibria are represented on P-T diagrams (Fig. 5). These diagrams were constructed by taking into consideration all the experimental data points available for each series of melt H_2O concentration (except charge #10, see above). Liquidus phase assemblages are divided into three groups: (1) ol + sp, (2) ol + sp + cpx and (3) cpx + opx ± sp. Plagioclase and garnet were not found. Spinel is present at the lowest pressures investigated (7.5 kbar, Table 2) but there is no sp + liquid field. Spinel is absent in a number of charges especially at high pressures (e.g., #24, 26 from the 1.5 wt.% H_2O series of experiments, Table 2; #8, 17 from the 4.5 wt.% H_2O experiments, Table 3). The 4-phase ol + cpx + opx + sp assemblage has been found only in charge #10, which, however, is thought to be out of equilibrium (see above).

In both phase diagrams (Fig. 5), the ol + sp assemblage is located at low pressures and the cpx + opx +/- sp assemblage at high pressures. The ol + cpx + sp field is found in an intermediate pressure domain and only in the 1.5 wt.% H_2O experiments. This assemblage was not detected in the 4.5 wt.% H_2O experiments, probably because of the smaller number of data points and larger spacing between experiments for this series of melt H_2O concentrations. At low pressure, olivine and spinel crystallize simultaneously below the liquidus where SEM observations show the presence of both isolated spinel crystals and spinel inclusions in olivine. At higher pressure, both cpx and opx (± sp) appear together on the liquidus. Neither a cpx + liquid nor an opx + liquid field has been found. For both series of melt H_2O concentrations, the proportion of cpx crystallizing on or near the liquidus largely exceeds that of opx. In detail, the cpx:opx ratio is about ~ 8:1 (by weight) for the 1.5 wt.% H_2O and ~ 4:1 for the 4.5 wt.% H_2O series of experiments, respectively. Thus, increasing the H_2O content of the melt (and varying the P-T-fO_2 conditions of the liquidus accordingly) significantly changes the relative proportions of cpx and opx crystallizing on the liquidus.

For the 1.5 wt.% H_2O phase diagram (Fig. 5), the high pressure liquidus (above that where olivine is a liquidus phase) and field boundaries delimiting the ol + cpx + sp phase field are well constrained. The low pressure liquidus is less well constrained. On Figure 5, it has been drawn with a slightly positive slope, in agreement with previous studies under anhydrous conditions (e.g., Gust and Perfit, 1987; Kushiro, 1987; Bartels et al., 1991; Draper and Johnston, 1992; Tatsumi et al., 1994). In contrast, the low pressure liquidus for the 4.5 wt.% H_2O phase diagram is drawn with a slightly negative slope (Fig. 5). This is because additional experiments (Macdonald et al., 1998; in preparation) constrain the liquidus temperature of

STV301 in presence of ~ 4.5 wt.% H_2O in the melt to be 1200°C at 4 kbar. In both diagrams, the intersection of the low and high pressure liquidus fields defines multiple saturation points where the study composition would be simultaneously saturated with an ol + cpx + opx + sp phase assemblage. These points are located at 1235 °C, 11.5 kbar and 1185 °C, 16 kbar for 1.5 and 4.5 wt.% H_2O in the melt respectively, (Fig. 5). In terms of phase equilibria, varying the melt H_2O concentration mainly changes the P-T location of the multiple saturation points.

4.6. Phase Compositions

Olivine compositions range between $Fo_{92.4}$ and $Fo_{89.9}$ in the 1.5 wt.% H_2O series of experiments, and between $Fo_{92.3}$ and $Fo_{92.1}$ in the 4.5 wt.% H_2O series of experiments (Tables 4, 5). The Fe/Mg olivine-melt partition coefficient $(Fe/Mg)_{ol}/(Fe/Mg)_{glass}$ is 0.32 ± 0.03 for 1.5 wt.% H_2O (calculated with glass FeO concentrations), indistinguishable from that for 4.5 wt.% H_2O (0.31 ± 0.02). Values identical within error were found in the recent literature for comparable compositions and P-T conditions (0.26 to 0.30, Hirose and Kawamoto, 1995; 0.34 ± 0.01, Gaetani and Grove, 1998; 0.34 ± 0.01, Falloon and Danyushevsky, 2000). The achievement of consistent Fe-Mg olivine-melt partition coefficient provides an a posteriori verification of the fO_2 determinations since the Kd calculations use melt FeO concentrations computed from experimental fO_2 (see above).

Orthopyroxenes ($Wo_{2.7\ to\ 4.9}En_{81.8\ to\ 87}Fs_{10.2\ to\ 13.8}$) have elevated Al_2O_3 (6.8 to 10.6 wt.%), Al^{IV} (0.16 to 0.23 pfu, 6 O basis) and Al^{VI} (0.12 to 0.21 pfu). The TiO_2 contents are < 0.3 wt.%. Orthopyroxenes from the 4.5 wt.% H_2O series of experiments tend to be slightly richer in En, and poorer in Wo, Al_2O_3 and TiO_2 than those from the 1.5 wt.% H_2O series of experiments (Tables 4, 5). The Fe/Mg partition coefficient between orthopyroxene and melt is 0.34 ± 0.04, in agreement with results from recent literature (0.32 ± 0.02, Gaetani and Grove, 1998; 0.31 ± 0.02, Falloon and Danyushevsky, 2000).

Clinopyroxenes ($Wo_{36\ to\ 42.9}En_{49.7\ to\ 56.2}Fs_{7.1\ to\ 12.2}$) are Ca-rich with Wo contents increasing from the 1.5 to the 4.5 wt.% H_2O experiments (Gaetani et al., 1993). They have high Al_2O_3 (8.0 to 11.0 wt.%), Al^{IV} (0.18 to 0.23 pfu, 6 O basis) and Al^{VI} (0.15 to 0.25 pfu). TiO_2 contents are ~ 0.5 wt.%. Na_2O concentrations (0.55 to 1.18 wt.%) increase with pressure (Tables 4, 5). Clinopyroxenes from this study have a substantial proportion of Fe present as Fe^{3+} ($Fe^{3+}/\Sigma Fe$ = 22% on average in the 1.5 wt.% H_2O experiments, 30% in the 4.5 wt.% H_2O experiments; Fe^{3+} in cpx calculated from Lindsley, 1983). The Fe/Mg partition coefficient between clinopyroxene and melt, calculated with Fe in cpx = Fe^{2+} (i.e., as for orthopyroxene), is 0.45 ± 0.07 for the 1.5 wt.% H_2O and 0.49 ± 0.05 for the 4.5 wt.% H_2O experiments, respectively. These values are higher than results from the literature (e.g., 0.35 ± 0.05, Hirose and Kawamoto, 1995; 0.36 ± 0.04, Kinzler, 1997; 0.33 ± 0.02, Gaetani and Grove, 1998), although the data overlap in part. These high Fe-Mg clinopyroxene-melt partition coefficients are attributed to the oxidizing conditions of our experiments.

Spinels are Cr-Al spinels with Cr# (=Cr/(Cr + Al) ranging mostly between 20 and 28 and Mg# (calculated with Fe in sp = Fe^{2+}) between 63 and 81 (Tables 4, 5). In cpx-bearing crystal-rich charges from the 4.5 wt.% H_2O experiments (#11, 19), spinel has very low Cr# (<5, Table 5). The Cr/(Cr+Al) of the spinel in charge #10 is heterogeneous (Table 4). Average $Fe^{3+}/\Sigma Fe$ of spinel is 48% for the less oxidized 1.5 wt.% H_2O and 59% for the more oxidized 4.5 wt.% H_2O experiments (Fe^{3+} calculated by assuming 32 O and 24 cations in the formula unit). The Fe/Mg partition coefficient between spinel and melt is 0.98 ± 0.14 (calculated with Fe = Fe^{2+}, both in spinel and melt) or 0.69 ± 0.10 (calculated with Fe = ΣFe), the latter being in good agreement with values in the literature (0.54 ± 0.06, Kinzler, 1997; 0.60 ± 0.13, Gaetani and Grove, 1998).

The experimental glasses obtained in this study are all basaltic in composition and are characterized by a narrow range of SiO_2 contents, from ~ 48 to 50 wt.%. With progressive crystallization below the liquidus, glass SiO_2, Al_2O_3, TiO_2, Na_2O and K_2O increase whereas CaO, MgO and CaO/Al_2O_3 decrease. FeO_t increases slightly and glass Mg# decrease from 82 to 68 as crystallization proceeds. The most evolved glasses (i.e., the less MgO-rich) have SiO_2 contents near 50 wt.% and Al_2O_3 near 19 wt.% (Table 4) at 7.5 wt.% MgO. In other words, these glasses approach the composition of certain high-alumina basalts (Gust and Perfit, 1987; Draper and Johnson, 1992).

5. DISCUSSION

5.1. A Lherzolitic Mantle Source for the St. Vincent Arc Basalts

The experimental data presented in this paper demonstrate that STV301 is multiply-saturated on its liquidus with a lherzolitic mantle phase assemblage for both 1.5 and 4.5 wt.% H_2O in the melt. The compositions of near-liquidus phases are comparable to upper mantle minerals. This evidence suggests that the studied basalt is a product of partial melting of a lherzolitic mantle.

One may question how robust this conclusion is or, in other words, to what extent it is dependent of the conditions of the experiments. In this study, no experiments were performed under anhydrous conditions which leads to the question whether STV301 would be multiply-saturated with a lherzolite assemblage in absence of H_2O. Several high-MgO and picritic basalts compositionally close to STV301 have been found to be multiply-saturated with a lherzolite phase assemblage under dry conditions (e.g., Kushiro, 1987; Tatsumi et al., 1994 and see above). However, there are examples of similar high-MgO basalts which are not multiply-saturated under the same conditions, essentially because orthopyroxene is not present on the liquidus (Gust and Perfit, 1987; Bartels et al., 1991; Falloon et al., 1999). Although the absence of orthopyroxene on the liquidus has been attributed to its sluggish growth kinetics (Gust and Perfit, 1987; Falloon et al., 1999), it could alternatively be the consequence of the anhydrous conditions in those experiments. In the present study, the proportion of orthopyroxene (relative to clinopyroxene) crystallizing on the liquidus was found to decrease with decreasing the H_2O concentration in the melt. This observation is consistent with the fact that lherzolite melting reactions between ~ 10 to 20 kbar consume a larger proportion of opx under hydrous than under anhydrous conditions (Gaetani and Grove, 1998; Falloon and Danyushevsky, 2000). Therefore, experiments performed on anhydrous STV301 would be expected to have a modal proportion of opx

lower than in the 1.5 wt.% H_2O series of experiments. Orthopyroxene is, thus, expected to be either present in very small amounts or absent on the anhydrous liquidus of STV301, a conclusion consistent with observations for other similar high-MgO basalt compositions experimentally studied under dry conditions (Gust and Perfit, 1987; Bartels et al., 1991; Falloon et al., 1999). We stress the point that the absence of opx on the anhydrous liquidus of high-MgO basalts does not necessarily preclude an origin by melting of a lherzolite source under hydrous conditions.

It might be also questioned whether STV301 would remain multiply-saturated with a lherzolite phase assemblage for H_2O concentrations $>$ 4.5 wt.% in the melt, which is the maximum average melt H_2O concentration investigated in this study. Near-liquidus experiments by Nicholls and Ringwood (1973) have shown that the addition of water markedly increases the maximum pressure of olivine stability for olivine tholeiite compositions. The displacement of the multiple saturation point toward higher pressures, as observed in this study when increasing the melt H_2O concentration from 1.5 to 4.5 wt.%, is consistent with these results. Nicholls and Ringwood (1973) found olivine to be present on the liquidus of olivine tholeiite up to 27 kbar, 1090 °C for water-saturated conditions. Peridotite melting experiments have demonstrated that basaltic melts with H_2O concentrations between 7 and 12 wt.% can coexist with spinel lherzolite phase assemblages at around 1100 °C (Hirose and Kawamoto, 1995; Gaetani and Grove, 1998). Therefore, although the pressure/temperature coordinates of individual phase volumes likely depend on the H_2O content, increasing the melt H_2O concentration beyond 4.5 wt.% is not expected to change the liquidus phase assemblage for STV301. This will remain true until amphibole appears on the liquidus, presumably for temperatures $<$ 1100 °C (Nicholls and Ringwood, 1973; Hirose and Kawamoto, 1995; Gaetani and Grove, 1998). Note that for a STV301 melt to be multiply saturated with a lherzolitic assemblage at temperatures $\leq$ 1100°C, very high melt H_2O concentrations would be needed ($\geq\sim$ 10 wt.%) from the extrapolation of the multiple saturation P-T locus (Fig. 6). In the same way, previous studies have found that pressures $\geq$ 20 kbar are necessary for garnet to crystallize on the liquidus of olivine tholeiite compositions (Nicholls and Ringwood, 1973; Falloon et al., 1999). Although garnet has not been found in experiments from this study, it is expected that garnet replaces spinel on the STV301 liquidus above 20 kbar. Assuming a minimum pressure of 20 kbar for the crystallization of garnet in STV301, extrapolation of the multiple saturation P-T locus (Fig. 6) yields a minimum melt H_2O concentration of $\sim$ 7 wt.% for STV301 to be multiply saturated with a garnet lherzolite. Therefore, very high H_2O contents are needed for arc basalts to be last-equilibrated with a garnet-bearing lherzolite source. To summarize, we consider that the conclusion that STV301 is a product of partial melting of a lherzolitic source is robust, and does not depend significantly of the experimental melt H_2O concentrations imposed in this study.

5.2. H_2O Content of Primitive Arc Basalts from St. Vincent

The P-T conditions of multiple saturation for several high-MgO basalts are summarized on Figure 6. The data include results for both dry and hydrous conditions (only two studies available, including the present one) and are for basalts with MgO concentrations ranging between 10 and 13 wt.%. The two multiple-saturation points from this study are in quite good agreement with the data of Tatsumi (1982), both for basalts very close to each other in MgO content (12.5 and 11.7 wt.% MgO, respectively). Interpolation and extrapolation of the available multiple saturation points defines a P-T-H_2O locus along which STV301 would be in equilibrium with a lherzolitic phase assemblage. By increasing the H_2O concentration of the melt, conditions of multiple saturation progressively evolve toward lower temperatures and higher pressures. The data lead to the suggestion that the first 1 wt.% of added H_2O has quite a dramatic effect on the temperature of the multiple saturation point (Fig. 6), but comparatively little effect on the pressure.

5.2.1. Constraints from phase equilibria

Knowledge of the P-T-H_2O locus of Figure 6 permits discussion of the conditions of extraction of STV301 from its mantle source and to evaluate the H_2O content of primary melts. For a primary basalt such as STV301 to preserve its status as a primary magma, it is necessary that olivine crystallization is prevented or limited during magma ascent. Basaltic magma ascent in the subarc mantle is commonly viewed to occur via dykes and, consequently, is thought to involve little or no chemical reaction with wall-rocks, and is adiabatic (e.g., Tatsumi and Eggins, 1995). Basalt adiabats are shown on Figure 6, calculated with a constant slope of $dT/dP = 1$ °C/km (McKenzie and Bickle, 1988). Melt crystallization during ascent will be controlled by the relative slopes of the adiabat and of the low pressure liquidus (ol + liquid = liquid). If the slope of the low pressure liquidus is flatter than the adiabat, the melt may ascend unmodified. Alternatively, if the low pressure liquidus has a negative slope, olivine crystallization will occur during ascent. The former situation is the one expected for anhydrous basaltic melts while the latter is typical of hydrous systems, either H_2O-saturated or at equilibrium with a H_2O-rich fluid, which have liquidi with negative slopes (e.g., Nicholls and Ringwood, 1973; Yoder, 1976). It follows that a STV301 melt, if extracted from the mantle under anhydrous conditions, will have the ability to reach the surface unmodified and will thus preserve its primary geochemical characteristics. Conversely, if last-equilibrated with its mantle source under H_2O-rich conditions, a STV301 melt will crystallize a significant amount of ol during ascent and thus will not reach the surface unmodified. Therefore, phase equilibria considerations suggest extraction of STV301 from the mantle under relatively dry conditions. There should exist a maximum melt H_2O content beyond which the respective positions of the liquidus and adiabat prevent STV301 to reach the surface unmodified. However, for this maximum to be precisely defined, the slope of the low pressure liquidi would need to be better determined, both for 1.5 and 4.5 wt.% H_2O and for higher melt H_2O concentrations. Therefore, although it is not presently possible to more precisely constrain the H_2O content of STV301 from phase equilibria considerations, the general conclusion from the above analysis is that high-MgO and picritic arc basalts erupted at the surface must have been extracted from the mantle under relatively dry conditions.

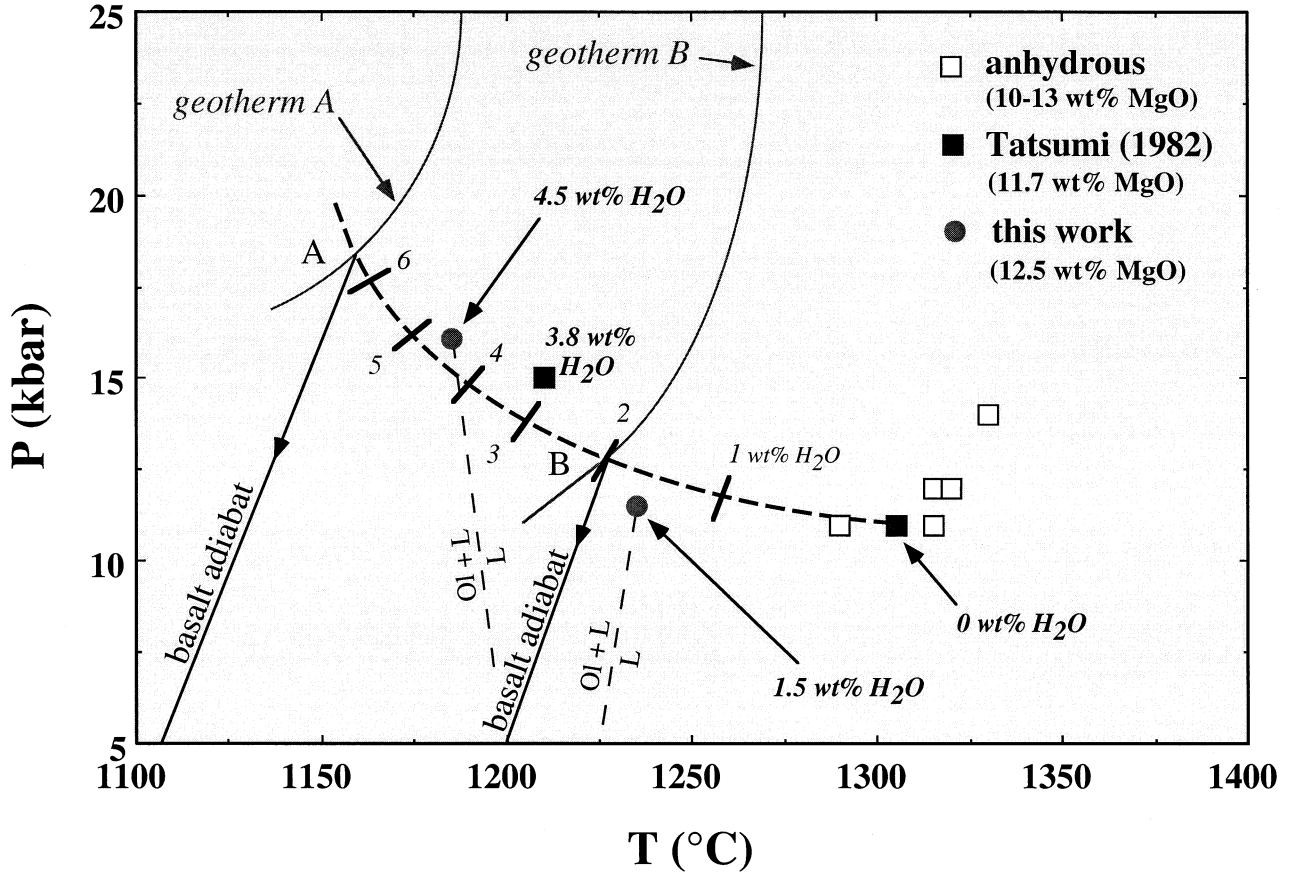

Fig. 6. P-T conditions of multiple saturation for several high-MgO and picritic arc basalts with MgO concentrations between ~ 10 and 13 wt.%. Source of data, anhydrous conditions: Kushiro (1987), Bartels et al. (1991), Draper and Johnston (1992), Tatsumi et al. (1994); hydrous conditions: Tatsumi (1982) and this study. The heavy dashed curve yields the P-T-H_2O in melt conditions of equilibrium of STV301 (12.5 wt.% MgO) with a spinel lherzolite source, constructed from the data of Tatsumi (1982) and of this study. Numbers along the curve are H_2O concentrations in the melt. A and B are two different examples of P-T-H_2O in melt conditions of last equilibration/extraction of the 12.5 wt.% MgO basalt with its mantle source. Adiabatic ascent paths are calculated from these two points (see text). The low pressure liquidi for STV301 with 1.5 and 4.5 wt.% H_2O in the melt (light dashed lines) are drawn for comparison with the adiabats. The two geotherms, drawn schematically through points A and B, illustrate the relation between the H_2O concentration of primary melts and the thermal regime of the mantle.

5.2.2. Evidence from glass inclusions

The direct analysis of water in glass inclusions trapped in phenocrysts has been a powerful way to constrain the H_2O concentration of primitive arc basalts. Glass inclusions in primitive arc magmas have average H_2O concentrations between 1.5 and 2.0 wt.% (Sobolev and Chaussidon, 1996), although H_2O contents up to 6 to 7 wt.% have sometimes been found (Sisson and Layne, 1993; Roggensack et al., 1997). No glass inclusion data are available for the primitive St. Vincent basalts. There is, however, a large body of data available for products of the 1979 eruption (Devine and Sigurdsson, 1983; Bardintzeff, 1992; Toothill, 1999). Basaltic inclusions trapped in olivine have average H_2O concentrations of ~3 wt.% (Macdonald et al., 2000). These glass inclusions do not represent primitive liquids but rather correspond to derivative compositions (i.e., MgO $\leq$ 3 to 4 wt.%). By taking 3 wt.% as the H_2O content of the derivative liquids and assuming that they represent products of 40% closed-system fractionation from parents such as STV301 (Sisson and Grove, 1993; Macdonald et al., 1998), a value of 1.8 wt.% H_2O is obtained for the primitive liquids. For comparison, Devine (1995) and Devine and Sigurdsson (1995) have suggested that the H_2O contents of relatively magnesian (close to primary) basalts of Grenada were 1 to 2 wt.% and that the melts parental to the Kick'em Jenny basalts initially contained ~ 2 wt.% H_2O. By using 2 wt.% as the H_2O concentration of primary STV301 melts, experimental data from this study suggest ~ 1230°C and ~ 13 kbar as the conditions of melt extraction from the mantle, corresponding to point B (Fig. 6). We conclude that the glass inclusion data provide evidence for relatively low melt H_2O concentrations in the primary mantle-derived magmas erupted at St. Vincent, consistent with the phase equilibria analysis above.

5.2.3. Other considerations

One interesting aspect of Figure 6 is the sensitivity of the temperature of multiple saturation on melt H_2O content. This

relationship could provide a method of evaluating the H_2O concentration of primary arc basalts, by determining their magmatic temperatures. In the case of the St. Vincent basalts, thermometric estimates for the most primitive rocks have yielded values between 1026 and 1130 °C (see above and Heath et al., 1998). A basalt adiabat consistent with the upper end of this temperature range must originate from the P-T-H_2O multiple saturation locus for STV301 at 1160 °C, 18.5 kbar, corresponding to a melt H_2O content of ~ 6.5 wt.% (point A, Fig. 6. This is a H_2O concentration markedly higher than suggested from the glass inclusion data and phase equilibria analysis. The most likely explanation of these conflicting observations is that the thermometric data significantly underestimate the liquidus temperature of STV301. The presence of cpx microphenocrysts (Heath et al., 1998) indicates that STV301 crystallized down to temperatures significantly below its liquidus. Therefore, to be applied to the determination of the melt H_2O concentration, a precise evaluation of the liquidus temperature of the primary magma is required.

Inversion of the incompatible trace element concentrations in STV301 could constitute another possible approach to estimating the water content of the source mantle and, by inference, of the basaltic products (Stolper and Newman, 1994). Recent studies have shown that there are three components reflected in the trace element and isotopic compositions of primitive basalts of the Lesser Antilles. These are the mantle wedge, an aqueous fluid and a component derived from subducted sediment (Thirlwall et al., 1996; Smith et al., 1996; Turner et al., 1996; Macdonald et al., 2000). Using the method of Turner et al. (1996), which assumes, *inter alia*, that Th in the subduction component is derived solely from the sediment component, we estimate sediment addition to the wedge to be around 6 wt.%. The proportion of fluid, estimated by mass-balance from the concentrations of the fluid-mobile elements such as Rb and Ba, varies from 30 wt.% to over 100 wt.%. Added uncertainties are assumptions about the water content of the fluid and the number of fluid pulses represented by the trace element abundances. It must be concluded, therefore, that the water content of the source mantle of STV301 cannot be sensibly constrained by this method. Concerning the REE, Macdonald et al. (2000) have shown that calc-alkaline magmas from the central islands of the Lesser Antilles arc bear no garnet signature which, given the conditions necessary for high-MgO basalts such as STV301 to be multiply-saturated with a garnet lherzolite assemblage on their liquidus (see above), would imply melt H_2O concentrations less than ~ 7 wt.% for the primary, mantle-derived, melts.

5.2.4. Summary

Several approaches have been used to constrain the H_2O content of primary, mantle-derived, melts from St. Vincent and elsewhere in the Lesser Antilles arc. Phase equilibria constraints, and in particular the necessity of preserving the mantle signature seen in high-MgO and picritic arc basalts, dictate relatively dry conditions of extraction from a spinel lherzolite mantle source. This conclusion is corroborated by the available glass inclusion data. Other approaches that may yield valuable results include use of the thermometric data and inversion of the incompatible trace element concentrations of primitive basalts. Although the conclusion is strongly in favour of extraction of relatively dry (~ 2 wt.% H_2O) primary melts, it is worth emphasizing that this range of H_2O concentration applies to primitive basalts that have the ability to erupt virtually unmodified at the surface. Because originally more hydrous melts will crystallize during ascent and will not be present unmodified at the surface, it should not be concluded that all primary arc basalts are extracted from their mantle source under similarly dry conditions. Therefore, determining the *range* of H_2O concentrations of primary basalts across a given arc really becomes the important issue. It remains to be evaluated whether relatively dry melts such as STV301 represent the exception rather than the rule.

5.3. Thermal Regime of the Mantle Wedge

Conditions of magma extraction in Figure 6 yield the P-T conditions of the mantle source and consequently constrain the mantle geotherm beneath the volcanic arc (e.g., Kushiro, 1987; Tatsumi et al., 1983; Tatsumi and Eggins, 1995). Two geotherms have been drawn schematically on Figure 6, each being constrained by the conditions of melt extraction discussed previously for STV301 (points A and B). The important point to be stressed is the direct relation between the H_2O content of primary melts and the temperature in the mantle wedge. Current thermal models for the subarc mantle are heavily influenced by experimental studies performed under anhydrous conditions (Fig. 6), which imply temperatures in excess of 1350 °C in the mantle wedge (Tatsumi et al., 1983; Kushiro, 1987; Tatsumi and Eggins, 1995). However, were primary basalts more hydrous, the mantle wedge could be much cooler, as illustrated in Figure 6.

5.4. Degrees of Melting and H_2O Content of the Mantle Source

Another possible approach is to constrain the H_2O content of primary arc melts from the viewpoint of the source, i.e., by using information available on the H_2O content of the subarc mantle. Melting in the mantle wedge commonly assumes a H_2O content of 0.2 wt.% (e.g., Kushiro, 1987), which would yield a basalt melt with 2 wt.% H_2O for 10% melting if it is assumed that H_2O is perfectly incompatible. However, more precise estimates of the H_2O content of the subarc mantle are now becoming available. The amount of subducted hydrous component (fluid and/or melt) added to the source region of arc basalts has been evaluated from oxygen isotopes (Eiler et al., 2000). From the $\delta^{18}O$ values of primitive arc lavas from Vanuatu-Fiji-New Caledonia, Eiler et al. (2000) concluded that their mantle sources were fluxed with ~0.5 to 1.0 wt.% (2.5 wt.% was suggested in some cases) of slab-derived hydrous component. By using the composition of the slab-derived component given by Eiler et al. (2000), this corresponds to a mantle H_2O content of ~0.45 to 0.9 wt.%. Although these H_2O estimates are model-dependant and may not be directly applicable to the Lesser Antilles arc, they constitute a useful basis for further discussion.

Since the inverse experimental approach is incapable of constraining the degree of melting at the level of magma extraction (e.g., Falloon et al., 1999), we have used the peridotite melting experiments of Hirose and Kushiro (1993) and

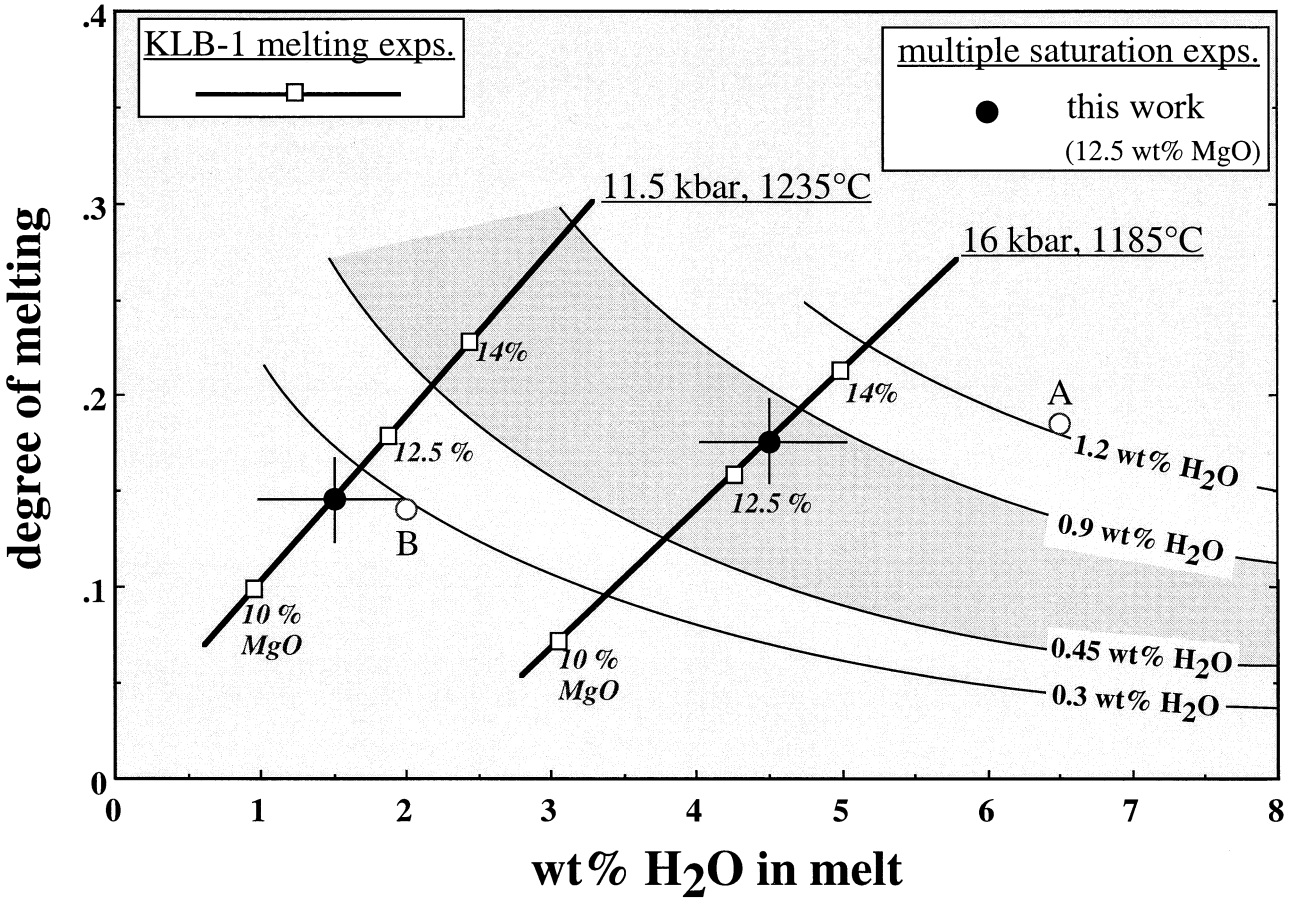

Fig. 7. Dependance of the degree of melting with the H_2O content of the melt for three MgO concentrations in the melt (10, 12.5, 14 wt.%) at 11.5 kbar, 1235 °C and 16 kbar, 1185 °C, i.e., for the P-T conditions of multiple saturation of STV301 with respectively 1.5 and 4.5 wt.% H_2O in the melt. The calculations are based on empirical regressions of the experimental data of Hirose and Kushiro (1993) and Hirose and Kawamoto (1995) on peridotite KLB-1 (see text). Note the small dependance of the degree of melting with the H_2O content for a given MgO content of the melt. Degrees of melting for STV301 are estimated from the KLB-1 partial melting grid by taking the melt H_2O contents appropriate for multiple saturation (1.5 and 4.5 wt.% H_2O). Note that the two STV301 points (12.50 wt.%, Table 1) plot close to the 12.5 wt.% MgO points calculated for the KLB-1 partial melts. A and B are the estimated degrees of melting for the two examples of multiple saturation conditions shown in Figure 6. The light curves are partial melting curves for 4 concentrations of H_2O in the mantle source (0.3, 0.45, 0.9, 1.2 wt.%), calculated by assuming that H_2O is perfectly incompatible during melting.

Hirose and Kawamoto (1995), both performed on the KLB-1 starting peridotite material, to estimate degrees of melting for STV301. Data on KLB-1 were selected for internal consistency because it is the only peridotite composition that has been subjected to systematic partial melting experiments under both anhydrous and hydrous conditions. The experimental degrees of melting and MgO concentrations of the partial melts (recalculated on an anhydrous basis) have been fitted with two empirical quadratic equations, each being a function of pressure, temperature and melt H_2O content. Degrees of melting and MgO concentrations of partial melts calculated with our regressions are within 15 and 6% relative, respectively, of the experimental values. These regressions enable the degree of melting and MgO content of the partial melt to be calculated for any set of P, T, H_2O in melt conditions covered in the studies of Hirose and Kushiro (1993) and Hirose and Kawamoto (1995).

A STV301 melt with 1.5 and 4.5 wt.% H_2O is in equilibrium with a spinel lherzolite at 11.5 kbar, 1235°C and 16 kbar, 1185°C, respectively. Under these conditions, degrees of melting calculated with the KLB-1 regression are 14.6 and 17.7%, and the calculated MgO concentrations of partial melts are 11.47 and 12.98 wt.%, respectively (Fig. 7). The fact that the MgO concentrations calculated for the KLB-1 partial melts and of STV301 (12.50 wt.%, Table 1) agree within 8% or better lends confidence to the approach and indicates that KLB-1 can, in first approximation, be taken as a model peridotite source for STV301. One aspect of general significance in Figure 7 is that degrees of melting are nearly constant along the multiple saturation P-T-H_2O in melt path (Fig. 6). This comes directly from the results of Hirose and Kawamoto (1995), which show degrees of melting to be almost independant of the H_2O content for a given MgO content of the melt. Therefore, the melt MgO concentration is a very robust indicator of the degree of melting, even in presence of water. The results (Fig. 7) suggest a degree of melting of 14 to 18% for STV301 (assuming a H_2O

concentration comprised between 1.5 and 4.5 wt.% in the melt), consistent with previous estimates based on trace elements (Heath et al., 1998).

Different contours for the H_2O concentration of the mantle source are also shown in Figure 7. The calculations assume perfectly incompatible behavior of H_2O during melting. For illustration purposes, two of the H_2O concentrations (0.3 and 1.2 wt.% H_2O) generate contours that pass very close to the points A and B (Fig. 6). For a STV301 melt to be extracted under conditions of point B, the mantle source would have to contain less than 0.3 wt.% H_2O (Fig. 7), which seems perfectly feasible if 0.2 wt.% is taken as the H_2O content of normal subarc mantle (Kushiro, 1987). If extracted under conditions represented by A, a mantle source distinctly more hydrous (1.2 wt.% H_2O) would be required. It remains to be established whether such amounts of H_2O are realistic for the Lesser Antilles subarc mantle, especially considering that the low rate of subduction in the arc (Macdonald et al., 2000) would limit the amount of subducted hydrous component added to the source region. For a mantle source with H_2O contents between 0.45 and 0.9 wt.% (see above and Eiler et al., 2000), H_2O concentrations between $\sim$ 2.5 to $\sim$ 5.5 wt.% would be expected for a melt with 12.5 wt.% MgO (Fig. 7). Therefore, if this range of source H_2O concentrations is accepted for the Lesser Antilles subarc mantle, it is in fact quite possible that some high-MgO primary melts have H_2O concentrations as high as 5.5 wt.%, i.e., well exceeding that of STV301 (i.e., $\sim$ 2 wt.% H_2O).

6. CONCLUSIONS

1. High-pressure piston-cylinder experiments have been conducted on a sample of primitive high-MgO basalt from St. Vincent, Lesser Antilles arc, under both oxidized and hydrous conditions. The experimental results demonstrate that the composition studied is multiply-saturated on its liquidus with a spinel lherzolite phase assemblage, at 1235 °C, 11.5 kbar for 1.5 wt.% H_2O in the melt, and at 1185 °C, 16 kbar for 4.5 wt.% H_2O in the melt. The composition of the liquidus mineral phases is similar to typical upper mantle minerals. This observation demonstrates that the basalt may represent a primary melt extracted from the subarc mantle.
2. Constraints from phase equilibria, glass inclusion data, and estimates of degrees of melting and of H_2O contents of the mantle source all favor extraction of the basalt under relatively dry conditions ($\sim$ 2 wt.% H_2O), at temperatures $\sim$ 1230 °C and pressures $\sim$ 13 kbar in the Lesser Antilles subarc mantle. However, this does not imply that all primary basalts in the Lesser Antilles arc necessarily were extracted under these conditions because only the driest melts will erupt. The more hydrous melts will crystallize during ascent and can not appear unmodified at the surface. Determination of the *range* of H_2O concentrations of primary basalts across a given arc remains an important issue which, to be implemented, requires a broader perspective on both derivative (high-alumina basalts and basaltic andesites, amphibole-bearing gabbroic cumulates, Macdonald et al., 2000; Pichavant et al., 2002) and primitive magmatic products, as well on the H_2O concentration of the mantle source.
3. Although this study has placed tight constraints on the conditions of extraction of primary basaltic melts, it is important to point out that the detailed conditions of melt generation in the mantle remain unexplored. Macdonald et al. (2000), for example, proposed that the various magmatic suites in the Lesser Antilles have all been derived from picritic, silica-undersaturated magmas. A view that would be more consistent with the new experimental results is that the different suites originated from compositionally distinct mantle melts.

Acknowledgments—This study was supported by PICS no. 419 between CNRS and the Carnegie Institution of Washington and partially by NSF grants EAR-961443 and EAR-9901886 to BOM. MP wants to acknowledge the members of the Geophysical Laboratory for making his 1997 stay both enjoyable and scientifically stimulating. Michel Champenois, Marc Chaussidon and Etienne Deloule (CRPG) are thanked for their help with the ion microprobe analyses at Nancy. This study benefited from discussions with Gaëlle Prouteau and Bruno Scaillet. Reviews by David Draper and an anonymous reviewer led to improvement of the manuscript.

Associate editor: F. J. Ryerson

REFERENCES

Albarède F. (1995) Introduction to Geochemical Modelling. Cambridge University Press, Cambridge.

Baker M. B., Grove T. L. and Price R. (1994) Primitive basalts and andesites of the Mt. Shasta region, N. California: products of varying melt fraction and water content. *Contrib. Mineral. Petrol.* **118,** 111–129.

Ballhaus C., Berry R. F. and Green D. H. (1991) High pressure experimental calibration of the olivine-orthopyroxene-spinel oxygen barometer: implications for the oxidation state of the upper mantle. *Contrib. Mineral. Petrol.* **107,** 27–40.

Bardintzeff J.-M. (1992) Magma mixing processes in volcanic contexts, a thermodynamic approach with the examples of St. Vincent Soufrière Volcano, West Indies and Cerro Chiquito, Guatemala. *Terra Nova* **4,** 553–566.

Bartels K. S., Kinzler R. J. and Grove T. L. (1991) High-pressure phase relations of primitive high-alumina basalts from Medecine Lake Volcano, northern California. *Contrib. Mineral. Petrol.* **108,** 253–270.

Behrens H., Romano C., Nowak M., Holtz F. and Dingwell D. B. (1996) Near-infrared determination of water species in glasses of the system $MAlSi_3O_8$ (M = Li, Na, K): an interlaboratory study. *Chem. Geol.* **128,** 41–63.

Brooker R., Holloway J. R. and Hervig R. (1998) Reduction in piston-cylinder experiments: the detection of carbon infiltration into platinum capsules. *Am. Mineral.* **83,** 985–994.

Brown G. M., Holland J. G., Sigurdsson H., Tomblin J. F. and Arculus R. J. (1977) Geochemistry of the Lesser Antilles island arc. *Geochim. Cosmochim. Acta.* **41,** 785–801.

Carmichael I. S. E. (1991) The redox states of basic and silicic magmas: a reflection of their source region? *Contrib. Mineral. Petrol.* **106,** 129–141.

Chou I.-M. (1987) Oxygen buffer and hydrogen sensor techniques at elevated pressures and temperature. In *Hydrothermal Experimental Techniques* (eds. H. L. Barnes and G. C. Ulmer), pp. 61–99. John Wiley, New York.

Danyuschevsky L. V. and Sobolev A. V. (1996) Ferric-ferrous ratio and oxygen fugacity calculations for primitive mantle-derived melts: calibration of an empirical technique. *Mineral. Petrol.* **57,** 229–241.

Deloule E., Paillat O., Pichavant M. and Scaillet B. (1995) Ion microprobe determination of water in silicate glasses: methods and applications. *Chem. Geol.* **125,** 19–28.

Devine J. D. (1995) Petrogenesis of the basalt-andesite-dacite association of Grenada, Lesser Antilles island arc, revisited. *J. Volcanol. Geotherm. Res.* **69,** 1–33.

Devine J. D. and Sigurdsson H. (1983) The liquid composition and

crystallization history of the 1979 Soufrière magma, St. Vincent. *J. Volcanol. Geotherm. Res.* **16,** 1–31.

Devine J. D. and Sigurdsson H. (1995) Petrology and eruption styles of Kick'em Jenny submarine volcano, Lesser Antilles island arc. *J. Volcanol. Geotherm. Res.* **69,** 35–58.

Devine J. D., Gardner J. E., Brack H. P., Layne G. D. and Rutherford M. J. (1995) Comparison of microanalytical methods for estimating H_2O contents of silicic volcanic glasses. *Am. Mineral.* **80,** 319–328.

Draper D. S. and Johnson A. D. (1992) Anhydrous PT phase relations of an Aleutian high-MgO basalt: an investigation of the role of olivine-liquid reaction in the generation of arc high-alumina basalts. *Contrib. Mineral. Petrol.* **112,** 501–519.

Eggins S. (1993) Origin and differentiation of picritic arc magmas, Ambae (Aoba), Vanuatu. *Contrib. Mineral. Petrol.* **114,** 79–100.

Eggler D. H., Mysen B. O. and Hoering T. C. (1974) Gas species in sealed capsules in solid media, high pressure apparatus. *Carnegie Inst. of Washington Yearbook.* **73,** 228–232.

Eiler J. M., Crawford A., Elliott T., Farley K. A., Valley J. W. and Stolper E. M. (2000). Oxygen isotope geochemistry of oceanic-arc lavas. *J. Petrol.* **41,** 229–256.

Falloon T. J., Green D. H., Jacques A. L. and Hawkins J. W. (1999) Refractory magmas in back-arc basin settings - Experimental constraints on the petrogenesis of a Lau basin example. *J. Petrol.* **40,** 255–277.

Falloon T. J. and Danyushevsky L. V. (2000). Melting of refractory mantle at 1.5, 2 and 2.5 GP a under anhydrous and H_2O-undersaturated conditions: implications for the petrogenesis of high-Ca boninites and the influence of subduction components on mantle melting. *J. Petrol.* **41,** 257–283.

Gaetani, G. A., Grove T. L. and Bryan W. B. (1993) The influence of water on the petrogenesis of subduction-related igneous rocks. *Nature.* **365,** 332–334.

Gaetani G. A. and Grove T. L. (1998) The influence of water on melting of mantle peridotite. *Contrib. Mineral. Petrol.* **131,** 323–346.

Green D. H. (1976) Experimental testing of "equilibrium" partial melting of peridotite under water-saturated, high pressure conditions. *Can. Mineral.* **14,** 255–268.

Gust D. A. and and Perfit M. R. (1987) Phase relations of a high-Mg basalt from the Aleutian island arc: implications for primary island arc basalts and high-Al basalts. *Contrib. Mineral. Petrol.* **97,** 7–18.

Heath E., Macdonald R., Belkin H. E. and Hawkesworth C. J. (1998) Magmagenesis at the Soufriere St. Vincent Volcano, Lesser Antilles arc. *J. Petrol.* **39,** 1721–1764.

Hirose K. and Kushiro I. (1993) Partial melting of dry peridotites at high pressures: determination of compositions of melts segregated from peridotites using aggregates of diamond. *Earth Planet. Sci. Lett.* **114,** 477–489.

Hirose K. and Kawamoto T. (1995) Hydrous partial melting of lherzolite at 1 Gpa—the effect of H_2O on the genesis of basaltic magmas. *Earth Planet. Sci. Lett.* **133,** 463–473.

Kawamoto T. and Hirose K. (1994) Au-Pd sample containers for melting experiments on iron and water bearing systems. *Eur. J. Mineral.* **6,** 381–385.

Kinzler R. J. (1997) Melting of mantle peridotite at pressures approaching the spinel to garnet transition: application to mid-ocean ridge basalt petrogenesis. *J. Geophys. Res.* **102,** 853–874.

Kress V. C. and Carmichael I. S. E. (1991) The compressibility of silicate liquids containing Fe_2O_3 and the effect of composition, temperature, oxygen fugacity and pressure on their redox states. *Contrib. Mineral. Petrol.* **108,** 82–92.

Kushiro I. (1987) A petrological model for the mantle wedge and lower crust in the Japanese island arcs. In *Magmatic Processes: Physicochemical Principles* (ed. B. O. Mysen), pp. 165–181. The Geochemical Society Special Publication No. 1, College Park.

Lindsley, D. H. (1983) Pyroxene thermometry. *Am. Mineral.* **68,** 477–493.

Macdonald R., Hawkesworth C. J. and Heath E. (2000) The Lesser. Antilles volcanic chain: a study in arc magmatism. *Earth Sci. Rev.* **49,** 1–76.

Macdonald R., Pichavant M. and Ertel W. (1998) Fractionation of arc basalts and the origin of the calc-alkaline suite. *Terra Nova Abstr. Suppl.* **1,** 36–37.

Marcelot G., Le Guen de Kerneizon M. and Bohn M. (1981) Zonation du nickel et du chrome dans les minéraux ferromagnésiens d'un basalte de Saint-Vincent (Petites Antilles); conséquences pétrogénétiques. *C. R. Acad. Sci. Paris.* **293,** 1079–1082.

Martel C., Pichavant M., Holtz F., Scaillet B., Bourdier J.-L. and Traineau H. (1999) Effects of fO_2 and H_2O on andesite phase relations between 2 and 4 kbar. *J. Geophys. Res.* **104,** 29453–29470.

Maurel C. and Maurel P. (1982) Etude expérimentale de l'équilibre Fe^{2+}-Fe^{3+} dans les spinelles chromifères et les liquides silicatés basiques coexistant. *C. R. Acad. Sci. Paris.* **285,** 209–215.

McKenzie D. and Bickle M. J. (1988) The volume and composition of melt generated by extension of the lithosphere. *J. Petrol.* **29,** 625–679.

Myers J. D. and Johnson A. D. (1996) Phase equilibria constraints on models of subduction zone magmatism. In *Subduction: Top to Bottom,* Geophysical Monograph **96,** pp. 229–249. American Geophysical Union, Washington.

Nicholls I. A. and Ringwood A. E. (1973) Effect of water on olivine stability in tholeiites and production of silica-saturated magmas in the island arc environment. *J. Geol.* **81,** 285–300.

Nye C. J. and Reid M. R. (1986) Geochemistry of primary and least fractionated lavas from Okmok volcano, Central Aleutians: implications for arc magma genesis. *J. Geophys. Res.* **91,** 10271–10287.

Patiño-Douce A. E. and Beard J. S. (1994) H_2O loss from hydrous melts during fluid-absent piston-cylinder experiments. *Am. Mineral.* **79,** 585–588.

Pichavant M. (1987) The effects of boron and water on liquidus phase relations in the haplogranite system at 1 kbar. *Am. Mineral.* **72,** 1056–1070.

Pichavant M., Martel C., Bourdier J.-L. and Scaillet B. (2002). Physical conditions, structure and dynamics of a zoned magma chamber: Mt. Pelée (Martinique, Lesser Antilles arc). *J. Geophys. Res.* in press.

Roggensack K., Hervig R. L., McKnight S. B. and Williams S. N. (1997) Explosive basaltic volcanism from Cerro Negro volcano: influence of volatiles on eruptive style. *Science.* **277,** 1639–1642.

Scaillet B. and Evans B. W. (1999) The June 15, 1991 eruption of Mount Pinatubo. I. Phase equilibria and pre-eruption P-T-fO_2-fH_2O conditions of the dacite magma. *J. Petrol.* **40,** 381–411.

Scaillet B., Pichavant M., Roux J., Humbert G. and Lefèvre A. (1992) Improvements of the Shaw membrane technique for measurement and control of fH_2 at high temperatures and pressure. *Am. Mineral.* **77,** 647–655.

Scaillet B., Pichavant M. and Roux J. (1995) Experimental crystallization of leucogranite magmas. *J. Petrol.* **36,** 663–705.

Sisson T. W. and Grove T. L. (1993) Temperatures and H_2O contents of low-MgO high-alumina basalts. *Contrib. Mineral. Petrol.* **113,** 167–184.

Sisson T. W. and Layne G. D. (1993) H_2O in basalt and basaltic andesite glass inclusions from four subduction-related volcanoes. *Earth Planet. Sci. Lett.* **117,** 619–635.

Smith T. E., Thirwall M. F. and MacPherson C. (1996) Trace-element and isotope geochemistry of the volcanic rocks of Bequia, Grenadine Islands, Lesser Antilles arc: a study of subduction enrichment processes. *J. Petrol.* **37,** 117–143.

Sobolev A. V. and Chaussidon M. (1996) H_2O concentrations in primary melts from supra-subduction zones and mid-ocean ridges. *Earth Planet. Sci. Lett.* **137,** 45–55.

Stolper E. M. and Newman S. (1994) The role of water in the petrogenesis of Mariana trough magmas. *Earth Planet. Sci. Lett.* **121,** 293–325.

Tatsumi Y. (1982) Origin of high-magnesian andesites in the Setouchi volcanic belt, southwest Japan II. Melting phase relations at high pressures. *Earth Planet. Sci. Lett.* **60,** 305–317.

Tatsumi Y. and Eggins S. M. (1995) Subduction Zone Magmatism. Blackwell, Cambridge.

Tatsumi Y., Sakuyama M., Fukuyama H. and Kushiro I. (1983) Generation of arc basalt magmas and thermal structure of the mantle wedge in subduction zones. *J. Geophys. Res.* **88,** 5815–5825.

Tatsumi Y., Furukawa Y. and Yamashita S. (1994) Thermal and geochemical evolution of the mantle wedge in the northeast Japan

arc 1. Contribution from experimental petrology. *J. Geophys. Res.* **99,** 22275–22283.

Thompson R. N. (1974) Primary basalts and magma genesis. *Contrib. Mineral. Petrol.* **43,** 317–341.

Thirlwall M. F. and Graham A. M. (1984) Evolution of high-Ca, high-Sr C-series basalts from Grenada, Lesser Antilles: the effect of intra-crustal contamination. *J. Geol. Soc. London.* **141,** 427–445.

Thirlwall M. F., Graham A. M., Arculus R. J., Harmon R. S. and MacPherson C. G. (1996) Resolution of the effects of crustal assimilation, sediment subduction and fluid transport in island arc magmas: Pb-Sr-Nd-O isotope geochemistry of Grenada, Lesser Antilles. *Geochim. Cosmochim. Acta.* **60,** 4785–4810.

Toothill J. (1999) The role of hydrous fluids in the generation of magmas in the Lesser Antilles. Unpub. Ph. D. thesis, University of Lancaster, 359 pp.

Truckenbrodt J., Ziegenbein D. and Johannes W. (1997) Redox conditions in piston-cylinder apparatus: the different behaviour of boron nitride and unfired pyrophyllite assemblies. *Am. Mineral.* **82,** 337–344.

Turner S., Hawkesworth C. J., van Calsteren P., Heath E., Macdonald R. and Black S. (1996) U-series isotopes and destructive plate margin magma genesis in the Lesser Antilles. *Earth Planet. Sci. Lett.* **142,** 191–207.

Yoder H. S. Jr. (1976) Generation of Basaltic Magma. National Academy of Sciences, Washington.